Spectral, tensor, and *ab initio* theoretical analysis of optical second harmonic generation from the rutile TiO_2(110) and (001) faces

Spectral, tensor, and *ab initio* theoretical analysis of optical second harmonic generation from the rutile TiO$_2$(110) and (001) faces

M Omote[1], H Kitaoka[1], E Kobayashi[1,4], O Suzuki[1], K Aratake[1], H Sano[1], G Mizutani[1,5], W Wolf[2] and R Podloucky[3]

[1] Japan Advanced Institute of Science and Technology, Tatsunokuchi, Ishikawa 923-1292, Japan
[2] Materials Design sarl, 44, avenue F-A Bartholdi, 72000 Le Mans, France
[3] Institute of Physical chemistry, University of Vienna, Liechtensteinstrasse 22A, A 1090 Vienna, Austria

E-mail: mizutani@jaist.ac.jp

Abstract
We give an overview of our recent experimental study on the optical second harmonic (SH) response of the rutile TiO$_2$(110) and (001) faces, and the analysis of these results by phenomenological electromagnetic theory using nonlinear susceptibility tensors and by *ab initio* theory using the self-consistent full potential linearized augmented plane-wave (FLAPW) method within the local-density approximation. Since bulk rutile TiO$_2$ has a uniaxial crystal structure of symmetry D$_{4h}^{14}$, the nonlinear optical response of its surface and bulk showed remarkable anisotropy. The TiO$_2$(110) face exhibited stronger reflected SH response when the incident electric field was directed parallel than perpendicular to the [001] axis, while the TiO$_2$(001) face exhibited relatively isotropic SH response. The anisotropy of the SH intensity patterns depended remarkably on the incident photon energy and the polarization combination. By using a phenomenological electromagnetic theory, we performed a simultaneous analysis of the SH intensity patterns from the (110) and (001) faces as a function of the sample rotation angle around its surface normal. As a result we could separate the contributions from the surface second-order and bulk higher-order nonlinear susceptibilities. We also found that the SH intensity spectra as a function of the SH photon energy depended strongly on the sample rotation angle and the polarization combination of the fundamental and SH light. The onset of the SH resonance of the TiO$_2$(110) face was located at $2\hbar\omega \sim 3.4$ eV when the induced nonlinear polarization was perpendicular to the surface. It was located at $2\hbar\omega \sim 3.2$ eV when the induced nonlinear polarization is parallel to the [001] direction in the surface

[4] Present address: Institute of Materials Structure Science, 1-1 Oho, Tsukuba, Ibaraki 305-0801, Japan.
[5] Author to whom any correspondence should be addressed.

plane. These onset energies were higher than the onset energy of the bulk linear absorption at 3.0 eV. On the other hand, the onset energy of the SH resonance of the (001) face was found at $2\hbar\omega \sim 3.0$ eV. A discussion is given on the physical meaning of the observed SH intensity spectra. Furthermore, an *ab initio* calculation of the nonlinear optical response from the $TiO_2(110)$ surface using the FLAPW method was performed. The calculated results agreed very well with the experimental SH intensity patterns and spectra. We found both from the phenomenological and *ab initio* calculation that the main SH response from the $TiO_2(110)$ surface originated from the Ti–O–Ti–O– zigzag chains on the $TiO_2(110)$ surface.

1. Introduction

Optical second harmonic (SH) spectroscopy has emerged as a new tool for the analyses of surfaces and interfaces of solid state materials [1–4]. By using the surface and interface specificity and resonance profile of second harmonic generation (SHG), we can find the distribution of surface and interface electronic levels on the energy scale in the band structure. By using the strong anisotropy of the SH response from asymmetric atomic bonds, we can find information on the surface and interface structures including those with adsorbates. This nonlinear optical technique offers us several significant advantages over the conventional surface spectroscopies. Unlike a method using electron or ion beams, it is free of material damage and contamination associated with charged particles. Sample surfaces in reaction in gaseous environment are accessible and so are the interfaces buried under optically transparent materials. Insulators can be studied without a problem of charging effects. For example, stoichiometric TiO_2 investigated in this study is an insulator and its surface electronic states cannot be studied in principle by ion or electron probes due to the charge up effect, while it can be studied with no problem by SH spectroscopy. Also in SH spectroscopy one can take advantage of the excellent spectral and temporal resolution given by the well-developed pulsed lasers or coherent light sources.

In spite of these advantages, the analysis of the anisotropy and the spectra of SH intensity of solid state material surfaces is not easy, and has not been performed widely. Only a limited number of attempts of systematic analyses have been made so far [5–8]. The separation of the contribution from the surface and bulk nonlinear susceptibility elements $\chi^{(2)}_{Sijk}$ and Γ_{ijkl} is difficult, because the number of these susceptibility elements is generally large. For media without bulk inversion symmetry, strong bulk dipolar SH response overwhelms the surface response, so we have to choose special configurations to suppress the bulk [9]. For centrosymmetric media like TiO_2 studied in this work, the strong bulk dipolar SH response is absent but higher-order electromagnetic multipoles cause a weak bulk SH radiation [10, 11].

The basic formulation of the analysis of SH intensity is straightforward, according to the framework developed in the textbook by Bloembergen [12]. However, for anisotropic materials like TiO_2 the analysis of the SH intensity is complicated. In an anisotropic medium, the incident electric field is split into two electromagnetic fields known as ordinary and extraordinary waves due to the birefringence effect. When we calculate its nonlinear optical response we must consider the birefringence effect both for incident and SH waves. Some of the works have gone into details of this treatment for anisotropic media [13–16]. However, there has been no example of a systematic and simultaneous analysis of SH intensity patterns and spectra for an
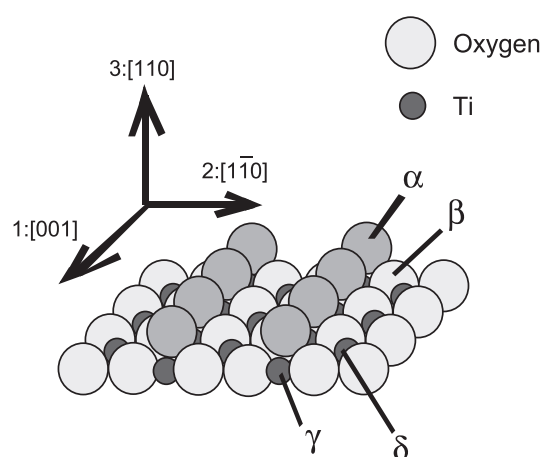
Figure 1. Model of the atomic arrangement of a clean TiO$_2$(110) surface. Bridging oxygen atoms (α-O) and the nearest neighbour titanium atoms (γ-Ti) form Ti–O–Ti–O– zigzag chains.

anisotropic nonlinear surface. In this study we give such a demonstration for titanium dioxide TiO$_2$, a material also well-known as a photo-catalyst working under UV light illumination.

The surface or interface electronic states of a photo-catalytic material are very important to investigate. For this purpose SH spectroscopy is a good candidate tool because a photo-catalyst usually works in a gaseous environment. In fact we have pointed out in our previous study that the SH intensity changes as the TiO$_2$ interface is illuminated with UV light [17, 18]. In order to analyse such a phenomenon and get information on the working electronic states, a thorough scrutiny and basic understanding of the nonlinear optical phenomena in this material not only with but also without UV light illumination is important. This study is focused on the latter case as a first step of such a study.

In our previous papers we performed a tentative analysis of the SH intensity patterns from rutile TiO$_2$(110) as a function of the azimuthal angle around its surface normal for the excitation photon energy at $\hbar\omega = 2.33$ eV [14]. From this analysis we have concluded that the observed SH light is generated mainly from the electric dipole polarization within a few atomic layers from the H$_2$O/rutile TiO$_2$(110) interface. The contribution of the bulk higher-order electromagnetic multipoles turned out to be not so large. We have also found that the SH intensity pattern drastically changed as the photon energy was changed [14, 19]. We suggested in the paper that the anisotropy of SH radiation is related to the anisotropy of the Ti–O–Ti–O– chains on the TiO$_2$(110) surface (figure 1).

In the present work we measured SH intensity spectra from the rutile TiO$_2$(110) face for various polarization configurations and sample rotation angle around its surface normal. In order to discuss the physical meaning of the spectra, we combined the analysis of the SH intensity spectra with that of the SH intensity patterns. We first performed analyses of the SH intensity patterns by a phenomenological theory at several photon energies. For this purpose we also needed the data from the TiO$_2$(001) face for comparison. We fitted the theoretical SH intensity patterns to the observed ones of the (110) and (001) faces simultaneously. Between the TiO$_2$(110) and (001) faces, the surface nonlinear susceptibilities are different but the bulk nonlinear susceptibility is common. For the analysis of the (001) face we also needed the incidence angle dependence of the SH intensity in order to remove the uncertainty in the fitting process. Then we gave an interpretation to the SH intensity spectra taking account of the obtained dominant susceptibility elements.

From the analysis of the SH intensity patterns and spectra it became clear that the surface Ti–O–Ti–O– chains contribute dominantly to the anisotropic SH radiation. In order to confirm

the validity of this model and to establish the strong way to analyse the SH response of the crystal surface in general, we have performed an *ab initio* calculation of the electronic states of the $TiO_2(110)$ surface and have calculated its SH intensity spectra and patterns [20].

This paper is organized as follows. In section 2 we show first the method of our sample preparation, our experimental set-up for the SH spectroscopy, and the methods of our phenomenological and *ab initio* theoretical analyses. In section 3 we show our experimental results of the SH intensity patterns and spectra of the $TiO_2(110)$ and (001) faces. In section 4 we show the results of our numerical analysis using the phenomenological theory with nonlinear susceptibility. In section 5 we show the results of our *ab initio* calculation of the SH intensity. In section 6, we evaluate the results of the phenomenological analysis, discuss the origin of the SHG from the TiO_2 faces, and consider the physical meaning of the observed SH intensity spectra.

2. Experimental details

2.1. Sample preparation

The samples were polished rutile $TiO_2(110)$ and (001) crystal faces (Nakazumi Crystal Laboratory). They were first annealed at 900 °C in oxygen atmosphere for 2 h to remove the bulk oxygen vacancies. Then, they were etched for 2 h in 5 mol l^{-1} NaOH aqueous solution at about 100 °C and subsequently in 2% HF aqueous solution for 1 min at room temperature, rinsed in pure water and dried naturally in the laboratory. The surface of the $TiO_2(110)$ face thus prepared was characterized by XPS and RHEED. We could identify a physisorbed H_2O layer on this face and it disappeared after annealing at 370 °C in vacuum. We could also see a carbon signal, but the carbon was judged to be adsorbed on the H_2O layer. Thus the prepared interface on the $TiO_2(110)$ bulk can be regarded as a $H_2O/TiO_2(110)$ interface and we call it 'the $TiO_2(110)$ face' in this paper. A RHEED pattern from this (110) face was taken in a vacuum chamber immediately after the chemical etching. They showed distinct (1×1) patterns. Asari *et al* have reported two types of (1×2) structures. A RHEED pattern from one of the (1×2) structures looked almost like a (1×1) pattern [21]. Thus, we cannot tell in principle whether the observed (1×1) RHEED patterns from our sample originate from the (1×1) or (1×2) structures on $TiO_2(110)$. On the other hand, Onishi *et al* have shown by LEED and STM analyses that the (1×1) structure is stable for annealing temperatures lower than 900 K, while the (1×2) structure is stable for annealing temperatures higher than 1150 K [22]. Considering that our chemically etched $TiO_2(110)$ surface had not experienced a temperature higher than 100 °C, the (1×1) surface is more probably realized under the H_2O physisorbed layer. Chung *et al* [23] also reported that the (110) 1×1 surface is quite inert and the (1×1) structure prepared in UHV remains after exposing it in air for 30 min. From these observations we believe that the interface we prepared was $H_2O/TiO_2(110)$ (1×1) [24]. The $TiO_2(110)$ face thus prepared looked pale yellow and transparent and was expected to have very few oxygen vacancies both in the bulk and at the interface.

'The $TiO_2(001)$ face' was prepared by the same process as the (110) face. This face is said to reconstruct to form (011) and (114) facets by annealing or to form a (1×1) surface by fracturing it at room temperature in vacuum [25]. Attempts were not made in the present work to clarify which of the above structures were realized on the prepared $TiO_2(001)$ face. This is because only the bulk contribution from the (001) face is important from the point of view of determining the nonlinear susceptibility of the (110) face. The surface contribution of the (001) face will become interesting in the future when the surface structures are characterized.
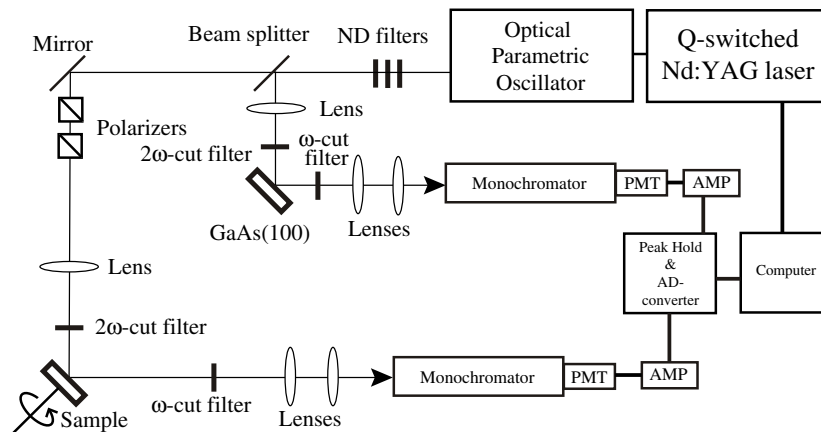
Figure 2. Block diagram of the experimental set-up for SHG measurements. OPO, BS, PMT, Amp, and A/D represent the optical parametric oscillator, beam splitter, photomultiplier tube, amplifier, and analogue-to-digital converter, respectively.

2.2. SHG measurement

The experimental set-up for the SHG measurements used in this study is schematically shown in figure 2. The light source of the fundamental frequency is an optical parametric oscillator (OPO) driven by a frequency-tripled Q-switched Nd:YAG laser with light pulses of duration 3 ns and repetition rate 10 Hz. The pulse energy was 0.5–1.0 mJ/pulse. The fundamental light beam from the OPO was passed through a coloured glass filter, a polarizer, and a lens, and was focused into a spot of 3 mm diameter on the sample surface. The incident angle was 45° from the surface normal. The reflected SH light beam in the specular direction was collected by lenses, passed through a coloured glass filter absorbing the fundamental light, a polarizer, lenses, and a monochromator, and was detected by a photomultiplier. The signal from the photomultiplier was digitally stored in a personal computer. To compensate for the temporal variation of the incident laser pulse power, we used a reference sample (GaAs(001) in air) and calibrated the signal intensity by taking the ratio of the intensities measured in the signal and reference channels. To compensate for the sensitivity variation of the optical system as a function of the wavelength, the SH intensity of a z-cut wedged quartz (α-SiO$_2$) plate was measured as a reference. The TiO$_2$(110), (001) and α-SiO$_2$(0001) samples were mounted on a sample stage with a sliding mechanism and their absolute SH intensities were measured in exactly the same optical configuration. For measuring the dependence of the SH intensity on the sample rotation angle around its surface normal, the sample was mounted on an automatic rotation stage with the surface normal set parallel to the rotating axis of the stage. All measurements were performed in air at room temperature.

2.3. Phenomenological analysis of the SH intensity patterns

We used Maxwell's equations with a nonlinear source term and calculated the amplitude of a second harmonic wave in a three-layered model shown in figure 3. In this model, layer 1 is a vacuum layer, layer 2 is the surface layer with second-order optical nonlinearity, and layer 3 is the bulk layer with a higher-order optical nonlinearity. The origin of the second-order nonlinearity in layer 2 is the breaking of symmetry in the direction normal to the surface by the discontinuity, reconstruction, or relaxation on the surface. We have assumed that layer 2
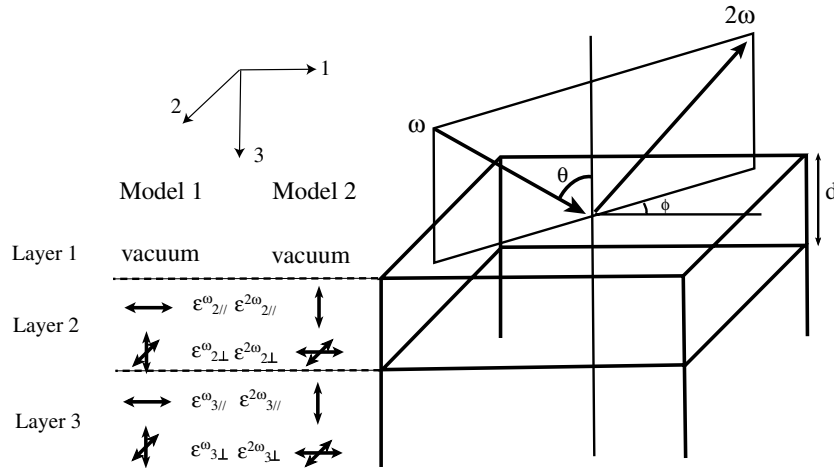
Figure 3. Dielectric model of a three-layer system used in the phenomenological analysis. The dielectric constants for the electric fields in the directions indicated by arrows are shown for the two models. Models 1 and 2 are for the TiO$_2$(110) and (001) faces, respectively. The *c*-axis or [001] direction of bulk TiO$_2$ crystal lies in directions 1 and 3 in models 1 and 2, respectively. In the appendix of this paper the coordinate $(1, 2, 3)$ is rewritten as (x, y, z) in order to avoid confusion.

is a thin layer with a uniform linear and nonlinear optical response. In fact the dielectric structure of the real surface layer is not so simple. The assumption is acceptable because the surface layer in this study is much thinner than the wavelength of light. In such a case the radiation from nonlinear polarizations can be regarded as that from one homogeneous dipole sheet. Layer 3 is the bulk region of a centrosymmetric crystal with D$_{4h}^{14}$ structure of rutile TiO$_2$. It does not have a second-order optical nonlinearity within a dipole approximation, but has a higher-order optical nonlinearity. Layers 2 and 3 are assumed to have a uniaxial dielectric response. Namely, dielectric function ε has anisotropic tensor components. In model 1 the *c*-axis in layer 3 lies in direction 1 and in model 2 it lies in direction 3.

The second-order nonlinear polarization in layer 2 is defined as

$$P_{S,i}^{(2)} = \Sigma_{ijk} \chi_{ijk}^{(2)} E_j E_k \tag{1}$$

using the phenomenological nonlinear susceptibility element $\chi_{ijk}^{(2)}$. E_j or E_k is the local electric field component of the incident light in layer 2. Following Guyot-Sionnest *et al* [26] we further define the surface nonlinear susceptibility in the substrate frame as $\chi_{Sijk}^{(2)}$. $\chi_{Sijk}^{(2)}$ is obtained by integrating $\chi_{ijk}^{(2)}$ over the surface layer (layer 2) as a function of depth. When some of the suffices of the susceptibility include the coordinate 3, the integrand is divided by the dielectric function for the electric field in direction 3 in layer 2 at the frequency of the corresponding photons. When we have a uniform linear and nonlinear dielectric response in layer 2 we will have

$$\chi_{S333}^{(2)} \equiv \frac{\chi_{333}^{(2)} d}{\varepsilon_{33}(2\omega)[\varepsilon_{33}(\omega)]^2} \tag{2}$$

$$\chi_{S3ij}^{(2)} \equiv \frac{\chi_{3ij}^{(2)} d}{\varepsilon_{33}(2\omega)} \qquad (i, j = 1, 2) \tag{3}$$

$$\chi_{Sij3}^{(2)} \equiv \frac{\chi_{ij3}^{(2)} d}{\varepsilon_{33}(\omega)} \qquad (i, j = 1, 2) \tag{4}$$

$$\chi^{(2)}_{Sijk} \equiv \chi^{(2)}_{ijk}d \qquad (i, j, k = 1, 2). \tag{5}$$

Coordinates 1 and 2 refer to the directions within the surface plane. For the (110) face the numbers 1, 2, and 3 represent the [001], [$\bar{1}$10], and [$\bar{1}\bar{1}$0] directions, respectively. For the (001) face the numbers 1, 2, and 3 represent the [100], [0$\bar{1}$0], and [00$\bar{1}$] directions, respectively.

The bulk nonlinear polarization in layer 3 is written as

$$P^{(2)}_{\mathrm{bulk},i} = \Sigma_{jkl}\Gamma_{ijkl}E_j\nabla_k E_l, \tag{6}$$

where Γ_{ijkl} is the higher-order nonlinear susceptibility [10]. E_j or E_l is the local electric field component of the incident beam in layer 3. The suffix i represents the direction of the nonlinear polarization at frequency 2ω, and the suffices j and l represent the directions of the incident electric field at frequency ω. They refer to the crystallographic axes x, y, and z in the crystal structure of TiO$_2$.

There are five and three independent surface nonlinear susceptibility elements $\chi^{(2)}_{Sijk}$ for the TiO$_2$(110) and (001) faces and they are shown later in figures 9 and 10, respectively. Here we have assumed that the structure of layer 2 has C$_{2v}$ and C$_{4v}$ symmetries for the TiO$_2$(110) and (001) faces, respectively. Layer 3 consists of the bulk rutile TiO$_2$ crystal. There are 11 non-zero bulk nonlinear susceptibility elements Γ_{ijkl} according to the symmetry of its crystal structure D$^{14}_{4h}$ and they are shown later in figure 11.

In order to calculate the SH intensity, the electric field amplitude of the incident laser beam in layers 2 and 3 is calculated first using Maxwell's equations as shown in the appendix A.1. Then the nonlinear polarizations in layers 2 and 3 are obtained by using equations (1) and (6). Finally, the amplitude of the electric field radiated by the nonlinear polarizations (1) and (6) are calculated by Maxwell's equations with nonlinear source terms as

$$\vec{\nabla}\times(\vec{\nabla}\times\vec{E}) + \frac{1}{c^2}\frac{\partial^2\stackrel{\leftrightarrow}{\varepsilon}\vec{E}}{\partial t^2} = -\frac{4\pi}{c^2}\frac{\partial^2\vec{P}_{\mathrm{NL}}}{\partial t^2} \tag{7}$$

as shown in the appendix A.2.

2.4. Method of ab initio calculation

The optical second harmonic (SH) response of the rutile TiO$_2$(110) surface was further studied by application of the self-consistent full potential linearized augmented plane-wave (FLAPW) method within the local-density approximation. *Ab initio* calculations of the surface SH response was performed for only a few surface systems of metal and elemental semiconductor such as Si [27]. In the case of TiO$_2$, there have been a lot of theoretical studies on the electronic states, the linear optical property [28, 29], the surface structure, and the surface electronic states [30–35], but there has been no calculation for surface SH response.

The details of the *ab initio* calculation will be published elsewhere [20, 36]. In short, for modelling the rutile TiO$_2$(110) 1 × 1 surface we applied a repeated slab construction. The structure of the relaxed TiO$_2$(110) surface was calculated by using the *ab initio* projector augmented wave (PAW) method within the generalized gradient approximation (GGA). The calculations of the ground state and the optical properties were made by application of the FLAPW method within the local-density approximation (LDA) of Hedin and Lundqvists [37]. Density, potential, and basis functions inside the atomic spheres were expanded into spherical harmonics up to $l_{\max} = 8$. Reciprocal-space integration was performed with the Gaussian smearing technique applying a width of 0.1 eV.

In the standard density-functional theory (DFT) calculation within the LDA, calculated band gaps are typically smaller than the experimental data and give rise to red-shifted calculated spectra. In order to improve the agreement of the calculation with the experimental data,

quasi-particle (QP) corrections have often been used. A scissors-like operator scheme was used for this purpose. The scissors-like operator makes all the unoccupied bands shift upward by a constant energy Δ_{QP} leaving the occupied bands unshifted. In this study the value of $\Delta_{QP} = 1.5$ eV was chosen to match the calculated absorption edge with the measured one.

The second-order nonlinear optical susceptibility tensor $\overleftrightarrow{\chi}_S^{(2)}$ was calculated referring to the formalism of [20, 36, 38, 39]. The imaginary part of the surface nonlinear susceptibility is defined by

$$
\begin{aligned}
\mathrm{Im}[\chi_{Sijk}^{(2)}(\omega)] = {} & \frac{2\pi}{\Omega}\left(\frac{e}{m\omega}\right)^3 \sum_{k\in SBZ}\left(\sum_{s\in V}\sum_{r\in C}\sum_{n\in C}\left(\frac{\tilde{p}_{sn}^i\{p_{nr}^j, p_{rs}^k\}}{E_{ns}-2E_{rs}}\right.\right. \\
& \times\left[\delta(E_{rs}-\hbar\omega)-2\delta(E_{ns}-2\hbar\omega)\right]+\frac{\tilde{p}_{nr}^i\{p_{rs}^k, p_{sn}^j\}}{E_{ns}+E_{rs}}\delta(E_{rs}-\hbar\omega)\bigg) \\
& -\sum_{s\in V}\sum_{l\in V}\sum_{n\in C}\left(\frac{\tilde{p}_{ln}^i\{p_{sl}^j, p_{ns}^k\}}{E_{nl}-2E_{ns}}[\delta(E_{ns}-\hbar\omega)-2\delta(E_{nl}-2\hbar\omega)]\right. \\
& \left.\left.+\frac{\tilde{p}_{sl}^i\{p_{ns}^k, p_{ln}^j\}}{E_{ns}+E_{nl}}\delta(E_{ns}-\hbar\omega)\right)\right)
\end{aligned}
\tag{8}
$$

where the braces indicate a symmetrization of the components j and k, Ω is the volume of the slab in the unit cell, e and m are the electronic charge and mass, and ω denotes the frequency of the incident photon. The notations s, r, n, and l indicate electronic states of the valence (V) or conduction (C) bands. E_{ns} denotes the direct energy gap between the one-electron energy levels n and s. The symbol $p_{nr}^j(k)$ denotes the matrix element of the momentum operator $\vec{p}$ defined by $p_{nr}^j = -i\hbar\langle\Psi_n(k)|\nabla_j|\Psi_r(k)\rangle$. The symbol $\tilde{p}_{nr}^i(k)$ marks the matrix element of the modified momentum operator for the emission of SH radiation defined by $\tilde{p} = \frac{1}{2}[S(z)\vec{p} + \vec{p}S(z)]$, where $S(z)$ is a function which decays inside the slab. In order to obtain the real part of the optical susceptibility, the Kramers–Kronig transformation was used. Using the nonlinear and linear susceptibilities thus obtained, the SH intensity was calculated according to the procedure described in section 2.3.

3. Measured SH intensity from the TiO$_2$(110) and (001) faces

3.1. SH intensity patterns from the TiO$_2$(110) face

In figure 4 we show the SH intensity from the TiO$_2$(110) face as a function of the sample rotation angle around its surface normal, for different polarization combinations and for different SH photon energies. In each pattern the SH intensity is plotted in the radial direction. The direction of the incident plane is defined in reference to the [001] axis as shown in figures 4(a) and (d). In each row the SH intensity patterns for four different polarization combinations are shown. As we go down to the lower rows, the SH photon energy $2\hbar\omega$ decreases and approaches the bulk band gap of TiO$_2$ (3.0 eV).

We see that the SH intensity shows symmetric patterns as a function of the sample rotation angle for every photon energy and polarization combination. According to the atomic structure of the TiO$_2$(110) interface of C$_{2v}$ symmetry, all the SH intensity patterns have two-fold symmetry. In order to check experimentally whether the observed SHG originates from the region within a few atomic monolayers from the interface or from the bulk, we have deposited SiO$_2$ of several nanometre thickness on the TiO$_2$(110) face and have measured the SH intensity patterns [40]. The observed patterns were different from those from the TiO$_2$(110) face, so
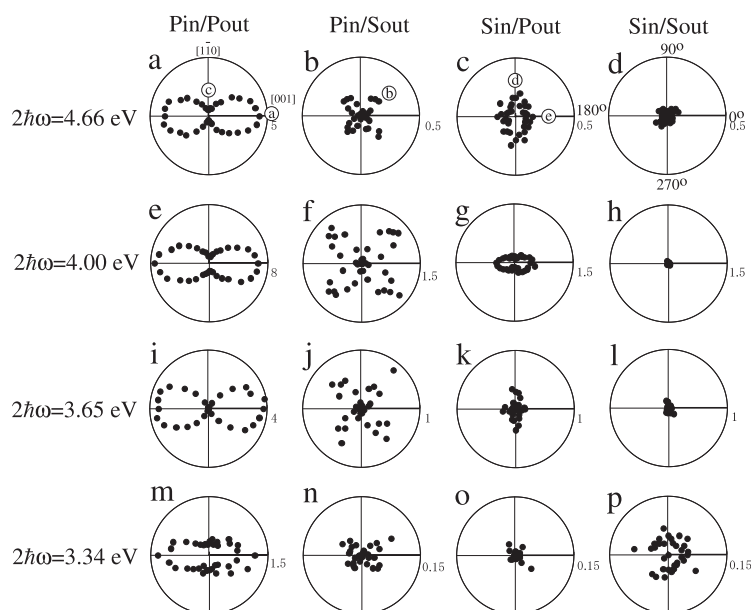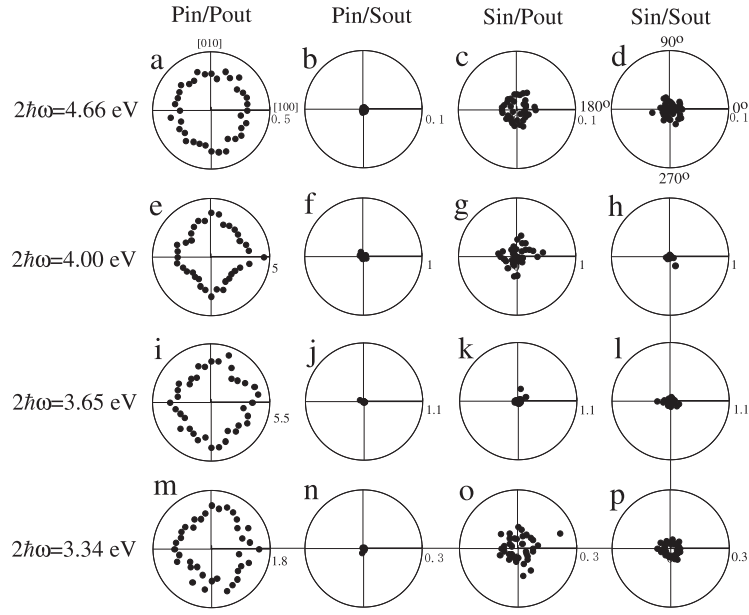
Figure 4. Measured SH intensity patterns from a TiO$_2$(110) face as a function of the sample rotation angle ϕ around its surface normal. The incident angle is 45°. The input and the output polarizations are shown in the figure, such as P_{in}/S_{out} for p-polarized input and s-polarized output. The SH photon energies are shown at the left. The SH intensity is plotted in the radial direction. The scale maximum of the intensity is shown in an arbitrary unit to the right of each pattern, and the patterns for the same SH photon energy are drawn in a common unit. The zero degree corresponds to the configuration when the plane of incidence includes the [001] direction on the sample. The lower-case letters from a to e in circles indicate the configurations for the spectroscopic measurements in figure 7.

that we can say that the SH light observed in figure 4 originates mainly from the region within a few monolayers from the TiO$_2$(110) interface. The pattern in figure 4(c) is especially sensitive to the SiO$_2$ deposition and is rotated by 90° by the deposition of SiO$_2$ layers.

Let us first look at the SH intensity pattern for p-polarized input and p-polarized output (P_{in}/P_{out}) light waves at the SH photon energy of $2\hbar\omega = 4.66$ eV in figure 4(a). We see that the SH intensity is higher when the incident plane is parallel to the [001] direction. In this configuration the incident electric field is in the plane containing the Ti–O–Ti–O– chains including the bridging oxygen atoms at the interface (figure 1).

Let us turn to the SH intensity patterns for the other polarization combinations in the first row (figures 4(b)–(d)). In P_{in}/S_{out} (figure 4(b)) and S_{in}/P_{out} (figure 4(c)) polarization combinations, the SH intensity is weak but we see anisotropic SH intensity patterns clearly. For the S_{in}/S_{out} polarization combination (figure 4(d)), the SH intensity is as low as the noise level.

We now turn to the SH intensity patterns for SH photon energies other than $2\hbar\omega = 4.66$ eV. When the SH photon energy $2\hbar\omega$ approaches that of the band gap of TiO$_2$ (3.0 eV) [41], the SH intensity becomes weaker and the SH intensity patterns change. All the patterns for P_{in}/P_{out} polarization combinations (figures 2(a), (e), (i), and (m)) consist of two lobes, but at $2\hbar\omega = 3.65$ eV the two-lobed pattern is narrow in the middle ($\phi = 90°$ and 270°). For the P_{in}/S_{out} polarization combination, the SH intensity has four lobes at all the SH photon energies. For the S_{in}/P_{out} polarization combination, the SH intensity is large when the incident plane is parallel to the [1$\bar{1}$0] direction at $2\hbar\omega = 4.66$ and 3.65 eV, while it is large when

Figure 5. Measured SH intensity patterns from the TiO$_2$(001) face as a function of the sample rotation angle ϕ around its surface normal. The incidence angle is 45°. The input and the output polarizations are shown in the figure, such as P_{in}/S_{out} for p-polarized input and s-polarized output. The SH photon energies are shown in the left. The SH intensity is plotted in the radial direction. The scale maximum of the intensity is shown in an arbitrary unit to the right of each pattern, and the patterns for the same SH photon energy are drawn in a common unit. The zero degree corresponds to the configuration when the plane of incidence includes the [100] direction on the sample.

the incident plane is parallel to the [001] direction at $2\hbar\omega = 4.00$ eV. At the photon energy of $2\hbar\omega = 3.34$ eV, the SH intensity is weak and we cannot find a pattern. For the S_{in}/S_{out} polarization combination, the signal at all the SH photon energies is below or comparable to the noise level.

The variation of the SH intensity patterns should reflect the variation of the shapes of the resonant surface electronic wavefunctions as a function of the photon energy, because the shapes of the electronic wavefunction determine the ratio of the magnitudes of the nonlinear susceptibility elements. The variation of the absolute SH intensity as a function of the photon energy will be shown in the SH intensity curves later in figure 7, at various combinations of polarizations and sample rotation angle ϕ, indicated by letters from a to e in small circles in figures 4(a)–(c).

3.2. SH intensity patterns from the TiO$_2$(001) face

In figure 5 we show the SH intensity patterns from the TiO$_2$(001) face as a function of the sample rotation angle. For all the four SH photon energies, the SH intensity is large for the P_{in}/P_{out} polarization combination, is non-zero for the S_{in}/P_{out} polarization combination, and is at a noise level for the other two polarization combinations. For the P_{in}/P_{out} polarization combination the SH response is almost isotropic as a function of the sample rotation angle, but a fourfold symmetric component is seen for $2\hbar\omega = 4.00$, 3.65, and 3.34 eV as shown in figures 5(e), (i), and (m). The ratios of the maximum SH intensities for the P_{in}/P_{out} polarization combination from the TiO$_2$(110) face to those from the TiO$_2$(001) face are listed in table 1.
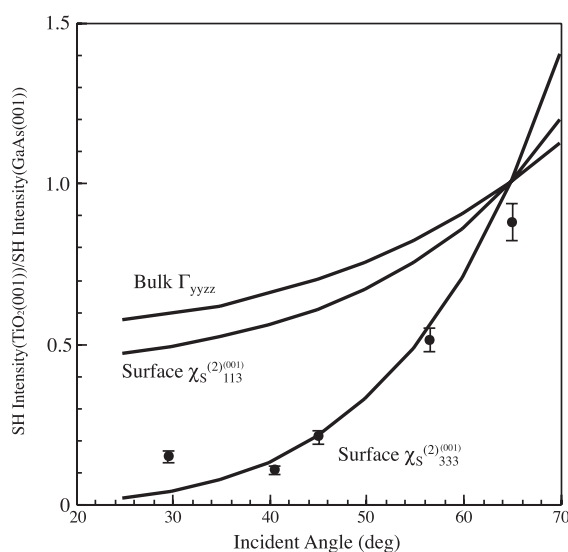
Figure 6. The SH intensity from the TiO$_2$(001) face as a function of the incident angle at the SH photon energy of $2\hbar\omega = 4.66$ eV. The dots with error bars represent SH intensity from the TiO$_2$(001) face divided by the SH intensity from the GaAs(001) as a function of the incident angle. The solid curves are calculated SH intensity for three important nonlinear susceptibility elements.

Table 1. The ratios of SH intensities from the H$_2$O/TiO$_2$(110) face to those from the H$_2$O/TiO$_2$(001) face.

SH photon energy $2\hbar\omega$ (eV)	(110):(001)
3.34	1.77:1
3.65	0.83:1
4.00	1.98:1
4.66	1.41:1

Figure 6 shows the SH intensity from the TiO$_2$(001) face as a function of the incident angle for the SH photon energy $2\hbar\omega = 4.66$ eV. These data are necessary in order to determine whether the surface or bulk contribution is dominant for the (001) face. In figure 6 dots with error bars represent SH intensity from the TiO$_2$(001) face divided by the SH intensity from the GaAs(001) as a function of the incident angle. The solid curves are calculated SH intensity for selected nonlinear susceptibility elements and will be described in detail later.

3.3. SH intensity from the TiO$_2$(110) and TiO$_2$(001) faces as a function of the photon energy

In figure 7 we show the SH intensity from the TiO$_2$(110) face as a function of the SH photon energy $2\hbar\omega$ for various polarization combinations and sample rotation angles ϕ. The polarization combination and the sample rotation angle adopted for each panel was indicated in figure 4 using the letters from a to e in circles. For example, the polarization combination and the sample rotation angle indicated by the symbol © in figure 4(a) gives the SH intensity spectrum in figure 7(c) as a function of the SH photon energy. The SH intensity between the photon energies $2\hbar\omega = 3.36$ and 3.64 eV was not measured because the light source we used, i.e. the optical parametric oscillator, does not oscillate in this photon energy region.

In all five spectra the SH intensity rises above the SH photon energy 3 eV, but the detailed onset energies of the SH intensity are different between the spectra. In figures 7(a) and (c)
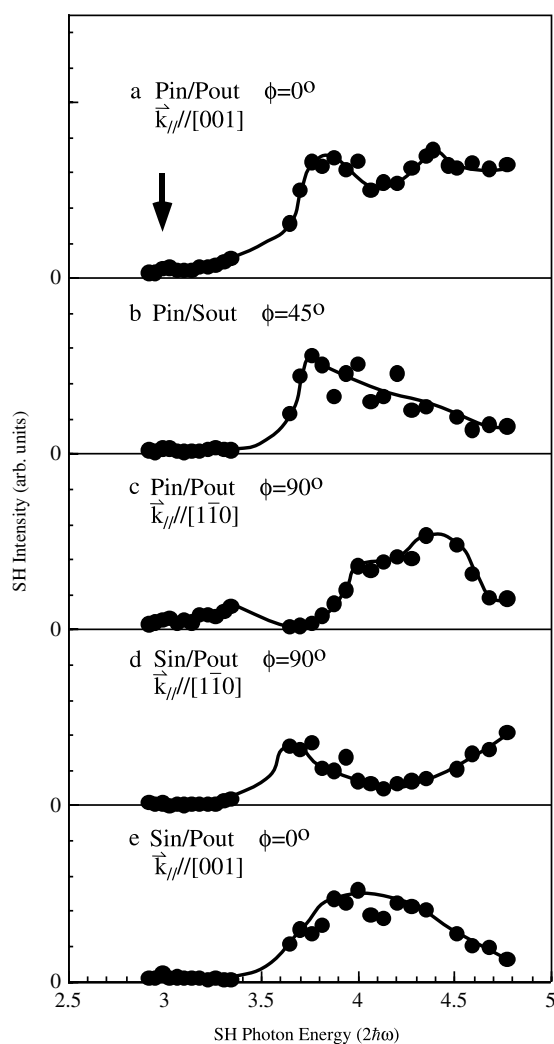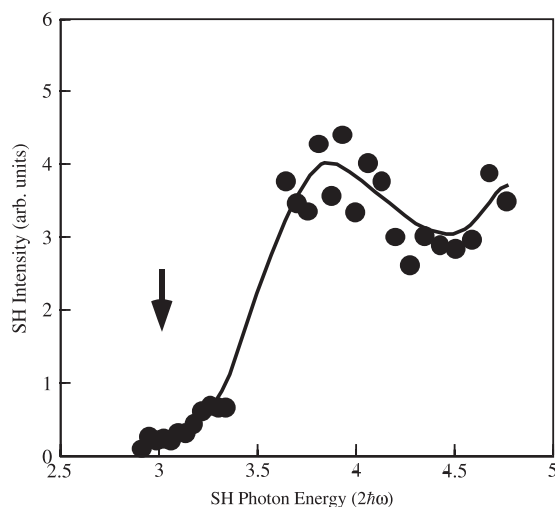
Figure 7. The reflected SH intensity from the rutile $TiO_2(110)$ face as a function of the SH photon energy $2\hbar\omega$ in air. The polarization combination and the sample rotation angle adopted for each panel are indicated in the figure and were also indicated in figure 4 using letters from a to e in circles. The solid curves are guides to the eye. The arrow indicates the band gap of the bulk rutile TiO_2.

the onset energy is around 3.2 eV. In figures 7(b), (d), and (e) the SH intensity is weak below $2\hbar\omega = 3.4$ eV and rises above this SH photon energy. This is consistent with the fact that figure 4(m) for $2\hbar\omega = 3.34$ eV exhibits finite SH intensity while figures 4(n) and (o) show very weak SH intensities. In figure 7(c) we find that the SH intensity is almost zero around $2\hbar\omega = 3.65$ eV for the P_{in}/P_{out} polarization combination and at $\phi = 90°$. This is consistent with the fact that the SH intensity is almost zero at $\phi = 90°$ and 270° in figure 4(i). In figure 7(d) we find that the SH intensity is lower around 4.1 eV than at 3.6 and 4.7 eV, while it is higher in figure 7(e). This is consistent with the fact that the SH intensity is higher at $\phi = 90°$ in figures 4(c) and (k), while it is higher at $\phi = 0°$ in figure 4(g).

In figure 8 we show the SH intensity from the $TiO_2(001)$ face as a function of the SH photon energy $2\hbar\omega$ for the P_{in}/P_{out} polarization combination and with the incident plane parallel to the [100] direction. We see that the SH intensity rises above the photon energy of $2\hbar\omega \sim 3.0$ eV. The SH intensity at 3.65 eV is roughly the maximum intensity in the spectra. This is in contrast to the fact that in figures 7(a) and (c) the SH intensity for the P_{in}/P_{out} polarization combination at $2\hbar\omega = 3.65$ eV is far below the maximum intensity in the spectra.

Figure 8. The reflected SH intensity from the rutile TiO$_2$ (001) face as a function of the SH photon energy $2\hbar\omega$ in air. The polarization combination is P_{in}/P_{out} and the plane of incidence is parallel to the [100] direction. The solid curve is a guide to the eye. The arrow indicates the band gap of the bulk rutile TiO$_2$.

ijk of $\chi^{(2)(110)}_{Sijk}$	Pin/Pout	Pin/Sout	Sin/Pout	Sin/Sout
113	1.392	0.221	0	0
223	1.953	0.345	0	0
311	2.269	0.004	1.043	0.002
322	2.277	0.004	2.002	0.003
333	51.165	0	0	0

Figure 9. SH intensity patterns obtained by theoretical calculation when one of the surface nonlinear susceptibility elements $\chi^{(2)(110)}_{Sijk}$ is set equal to a certain common value and all the other elements are set equal to zero. The SH intensity is normalized by the maximum intensity in each pattern, and the maximum intensity is shown below the pattern. The intensities are in arbitrary, but common, units. The suffices i, j, and k of the surface nonlinear susceptibility $\chi^{(2)(110)}_{Sijk}$ refer to the axis frame defined in figure 1.

ijk of $\chi^{(2)\,(001)}_{Sijk}$	Pin/Pout	Pin/Sout	Sin/Pout	Sin/Sout
113	◯ 2.016	0	0	0
311	◯ 2.295	0	◯ 1.486	0
333	◯ 32.773	0	0	0

Figure 10. SH intensity patterns obtained by theoretical calculation when one of the surface nonlinear susceptibility elements $\chi^{(2)(001)}_{Sijk}$ is set equal to a certain common value and all the other elements are set equal to zero. The SH intensity is normalized by the maximum intensity in each pattern and the maximum intensity is shown below the pattern. The intensities are in arbitrary, but common, units. As the suffices of the surface nonlinear susceptibility elements $\chi^{(2)(001)}_{Sijk}$, 1 indicates the direction [100] and 3 indicates the direction [001].

In order to check whether the signal observed in figures 7 and 8 is in one- or two-photon resonance with the surface electronic levels, we have measured sum frequency generation from the TiO$_2$(110) and TiO$_2$(001) faces (not shown). The results showed that all the signals were in two-photon resonance.

4. Results of the phenomenological analysis of the SH intensity patterns at $2\hbar\omega = 4.66$ eV

In this section we will carry out a numerical analysis of the observed SH intensity patterns from the TiO$_2$(110) and TiO$_2$(001) faces shown in figures 4 and 5 by a phenomenological electromagnetic theory using the second-order nonlinear optical susceptibilities as adjustable parameters.

Figures 9 and 10 show the calculated SH intensity patterns and the peak intensities from the dielectric structures of models 1 and 2 illustrated in figure 3 for the TiO$_2$(110) and (001) faces, respectively, when one of the five and three surface nonlinear susceptibility elements $\chi^{(2)(110)}_{Sijk}$ and $\chi^{(2)(001)}_{Sijk}$ is set equal to a common value and the other elements are all set equal to zero. Here, $\chi^{(2)(110)}_{Sijk}$ and $\chi^{(2)(001)}_{Sijk}$ are defined as the surface nonlinear susceptibility for the (110) and (001) faces, respectively. We used dielectric constants of TiO$_2$, $\varepsilon_\parallel(2.33$ eV$) = 8.821$ and $\varepsilon_\parallel(4.66$ eV$) = -7.409 + i13.24$ for the electric fields parallel to the [001] crystal axis, and $\varepsilon_\perp(2.33$ eV$) = 7.129$ and $\varepsilon_\perp(4.66$ eV$) = 3.165 + i8.15$ for the electric fields perpendicular to the [001] axis [42]. The patterns were calculated for all four combinations of the p- and s-polarized incidence and output. Figure 11 shows the calculated SH intensity patterns and the peak intensities from the dielectric structures of models 1 and 2, when one of the 11 Γ_{ijkl} elements is set equal to a common value and the other elements are all set equal to zero.

Now we fit the theoretical SH intensity patterns to those obtained in the experiment shown in figures 4 and 5. We calculated the linear combinations of the patterns in figures 9–11 in the complex plane with each pattern multiplied by the relevant nonlinear susceptibility element
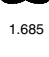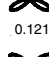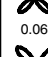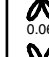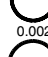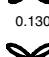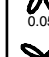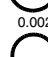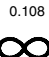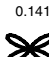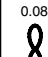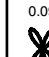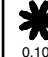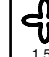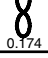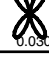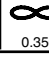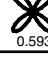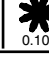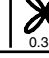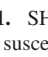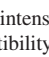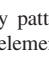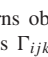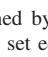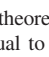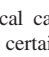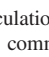
ijkl of Γ_{ijkl}	(110) [1̄10] → [001]				(001) [100] → [010]			
	Pin Pout	Pin Sout	Sin Pout	Sin Sout	Pin Pout	Pin Sout	Sin Pout	Sin Sout
xxxx	0.210	0.243	0.350	0.043	2.378	0.103	0.386	0.068
zzzz	1.092	0.078	0.040	0.045	0.001	0	0	0
yyzz	0.107	0.141	0.083	0.090	1.554	0	0	0
zzyy	1.685	0.121	0.061	0.069	0.002	0	0	0
zyyz	1.685	0.130	0.049	0.057	0.002	0	0	0
yzzy	0.108	0.141	0.083	0.090	1.553	0	0	0
yzyz	1.821	0.141	3.416	0.082	0.006	0	0	0
zyzy	0.125	0.131	1.045	0.075	0.596	0	0.383	0
xxyy	0.174	0.024	0.350	0.030	0.593	0.103	0.386	0.068
xyxy	9.340	0.733	0.350	0.027	0.593	0.103	1.544	0.068
xyyx	0.174	0.030	0.350	0.018	0.593	0.103	0.386	0.068

Figure 11. SH intensity patterns obtained by theoretical calculation when one of the surface nonlinear susceptibility elements Γ_{ijkl} is set equal to a certain common value and all the other elements are set equal to zero. The SH intensity is normalized by the maximum intensity in each pattern and the maximum intensity is shown below the pattern. The intensities are in arbitrary, but common, units. The suffices of the bulk nonlinear susceptibility Γ_{ijkl} refer to the crystallographic axis of the bulk rutile TiO₂.

$\chi_{Sijk}^{(2)(110)}$, $\chi_{Sijk}^{(2)(001)}$, or Γ_{ijkl} and then vary the nonlinear susceptibility elements as adjustable parameters. Generally, in fortunate cases, we can determine the nonlinear susceptibility elements from the best fit results of this fitting. However, since there are susceptibility elements giving similar patterns as seen in figures 9–11, we cannot determine the unique set of susceptibility elements. There is a considerable amount of arbitrariness in the determination of the set of the nonlinear susceptibility elements for these faces, and the fitting program shows unstable output.

In order to overcome this problem we should get further information from other index faces or the incident angle dependence of the SH intensity of the faces under study, in order to get the information of the dominant susceptibility elements [43]. In the present case, we measured the incident angle dependence of the SH intensity from the TiO₂(001) face as in figure 6, and determined whether the surface or bulk contribution is dominant in the SH radiation from the (001) face. We also reduced the number of adjustable susceptibility elements by making
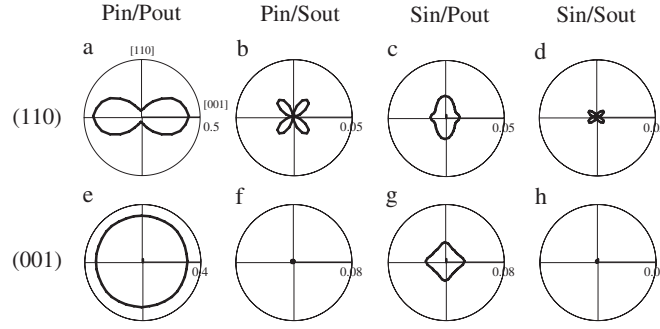
Figure 12. SH intensity patterns obtained by theoretical calculation fitted to the experimental data of figures 4(a)–(d) ((a)–(d)) and to those of figures 5(a)–(d) ((e)–(h)).

groups of the elements giving the same or similar SH intensity patterns, and by making only one member in each group an adjustable parameter in the fitting.

In figure 6 the SH intensity was measured relative to the bulk SH intensity from GaAs(100). We also show by solid curves the calculated SH intensity by selected nonlinear susceptibility elements from the structure model 2 divided by the calculated SH intensity from GaAs(100). The nonlinear susceptibility elements considered are $\chi_{S113}^{(2)(001)}$, $\chi_{S333}^{(2)(001)}$, and Γ_{yyzz}. The reason why we consider only the element Γ_{yyzz} among the Γ_{ijkl} is as follows. In figure 11 the bulk nonlinear susceptibility elements giving intense isotropic SH intensity patterns from the (001) face for the P_{in}/P_{out} polarization combination like that in figure 5(a) is Γ_{yyzz}, Γ_{yzzy}, and Γ_{zyzy}. Among these three elements Γ_{zyzy} does not make dominant contribution in figure 5(a) because the observed SH intensity in figure 5(c) is not so large compared with that in figure 5(a), unlike the corresponding patterns for Γ_{zyzy} in figure 11. Γ_{yzzy} gives the same patterns as Γ_{yyzz}, as is shown in figure 11 and also as is described later in equation (10). Thus we should only consider the Γ_{yyzz} element among the Γ_{ijkl}. Comparing the theoretical and experimental data in figure 6, it is clear that the $\chi_{S333}^{(2)(001)}$ element is the most dominant among the three susceptibility elements.

In order to reduce the number of the susceptibility elements, the following non-zero susceptibility elements are selected from the groups of the elements in the parentheses as

$$\Gamma_{zyyz}(\Gamma_{zyyz}, \Gamma_{zzyy}, \Gamma_{zzzz}) \tag{9}$$
$$\Gamma_{yyzz}(\Gamma_{yyzz}, \Gamma_{yzzy}), \tag{10}$$

and

$$\Gamma_{xxyy}(\Gamma_{xxyy}, \Gamma_{xyyx}). \tag{11}$$

In the present study we further assumed

$$\chi_{S113}^{(2)(001)} = 0, \qquad \Gamma_{zyzy} = 0 \tag{12}$$

from the above discussion on figure 6. We also assumed

$$\Gamma_{yzyz} = 0 \tag{13}$$

because we have found that the SH intensity in figure 4(c) is not due to the bulk response, as was mentioned in section 3.1.

In figure 12 we show the calculated SH intensity patterns fitted to the experimental data. The patterns in figures 12(a)–(d) reproduce the measured patterns in figures 4(a)–(d), while the patterns in figures 12(e)–(h) reproduce the measured ones in figures 5(a)–(d). We find that
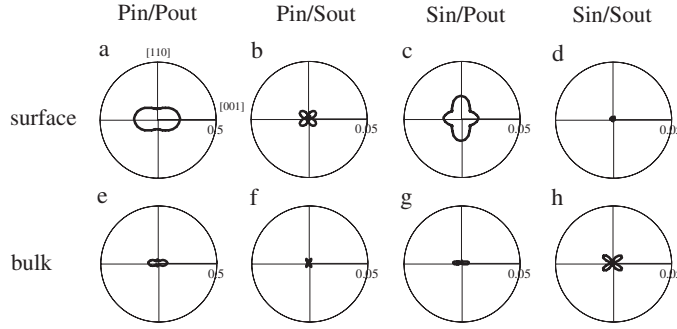
Figure 13. Calculated surface ((a)–(d)) and bulk ((e)–(h)) contributions in the SH intensity separated from the patterns in figures 12(a)–(d).

the calculation based on the phenomenological theory reproduces the experimental data very well. In figure 13, the calculated patterns in figures 12(a)–(d) are decomposed into the surface ((a)–(d)) and bulk ((e)–(h)) contributions. In the SH intensity patterns for all the polarization combinations except S_{in}/S_{out}, the surface contribution is dominant.

Further separating the calculated SH intensity patterns for the P_{in}/P_{out} polarization combination at $2\hbar\omega = 4.66$ eV into the contribution of each susceptibility element, we find that the contribution of the $\chi_{S113}^{(2)(110)}$ element is the largest, and then the $\chi_{S223}^{(2)(110)}$ and $\chi_{S333}^{(2)(110)}$ elements are the next largest in the SH intensity. The $\chi_{S113}^{(2)(110)}$ and $\chi_{S223}^{(2)(110)}$ elements contribute to the SH intensity for the P_{in}/S_{out} polarization combination. For the S_{in}/P_{out} polarization combination, the $\chi_{S311}^{(2)(110)}$ and $\chi_{S322}^{(2)(110)}$ elements contribute much, but the resulting SH intensity pattern is determined as a result of the interference between many susceptibility elements, so it is not easy to determine which elements dominate the observed SH intensity pattern. For the S_{in}/S_{out} polarization combination the bulk contribution (figure 13(h)) is larger than that from the surface (figure 13(d)), but this is a result of erroneous separation of the noise component.

Most of the signals from the TiO$_2$(001) face for the P_{in}/P_{out} polarization combination is assigned to the surface contribution, and the $\chi_{S333}^{(2)(001)}$ element was shown to contribute most dominantly to the SH intensity (not shown). This is consistent with the result in figure 6.

The SH intensity pattern in figure 5(c) is reproduced as a fourfold symmetric curve as shown in figure 12(g). The fourfold symmetric component is attributed to the bulk higher-order nonlinearity, because we see in figure 10 that no surface component gives a fourfold symmetric pattern. The fourfold symmetric component for the S_{in}/P_{out} polarization combination is mostly given by the Γ_{xxxx} and Γ_{xxyy} elements, while the isotropic component is given by the $\chi_{S311}^{(2)(001)}$ element.

The analysis of the SH intensity patterns in figures 4 and 5 for the SH photon energies $2\hbar\omega = 4.00$ and 3.65 eV gave similar results, and the dominant contribution of the SH intensity from the TiO$_2$(110) face for the P_{in}/P_{out} polarization combination came from the $\chi_{S113}^{(2)(110)}$ element. The dependence of the SH intensity pattern on the photon energy as seen in figures 4(c), (g), and (k) is very interesting, but we could not determine from this analysis which nonlinear susceptibility element is responsible for this pattern variation because many susceptibility elements contribute to the SH intensity for this polarization combination. The dominant susceptibility element will be analysed in a qualitative discussion in section 6.3.

At $2\hbar\omega = 3.34$ eV the fitting error was so large that we could not determine whether surface or bulk contribution was dominant. Since the SH intensity patterns in figure 5 show a fourfold symmetric component for the P_{in}/P_{out} polarization combination for the lower photon energies, the bulk contribution is judged to be stronger for the lower photon energies.
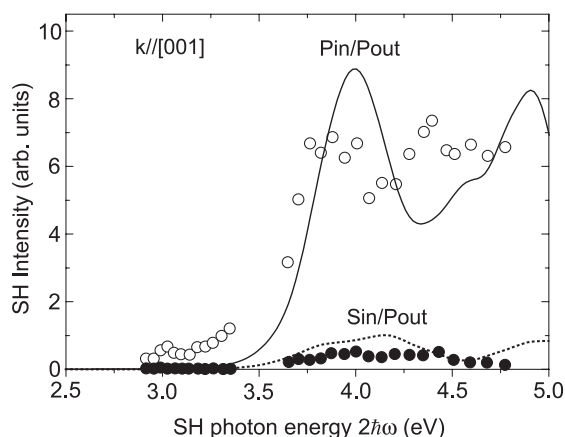
Figure 14. Calculated SH intensity as a function of the SH photon energy for P_{in}/P_{out} (solid curve) and S_{in}/P_{out} (dashed curve) polarization combinations for the relaxed $TiO_2(110)$ surface. The plane of incidence is parallel to the [001] direction. Empty and grey circles are the measured SH intensity and are the same data as those shown in figures 7(a) and (e). The scale of the measured data is adjusted to match the calculated data.
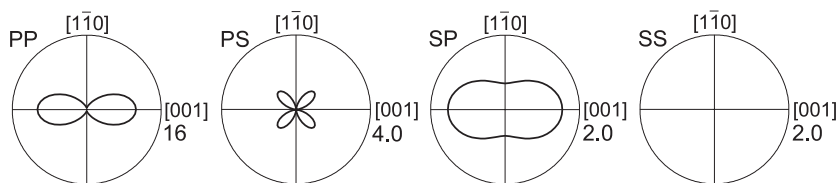
Figure 15. SH intensity as a function of the sample rotation angle ϕ around the surface normal at the SH photon energy $2\hbar\omega = 4.0$ eV obtained by the *ab initio* calculation. The scales in the radial direction are in an arbitrary but common unit.

5. Results of the *ab initio* calculation

Here we show the results of our recent *ab initio* calculation according to the procedure described in section 2.4 of the SH intensity from the $TiO_2(110)$ surface, and will compare the results with our experiment. Further details can be found in our future publication [20].

Firstly, we note that in the calculated density of states (DOS) of the relaxed surface two peaks assigned to the bridging oxygen α-O in figure 1 were seen at the top of the valence band and around the energy of -16 eV (not shown). The DOS of α-O has a peak at the energy of ~ 1 eV below the top of the valence band for the relaxed surface, while it was found just at the top of the valence band for the unrelaxed surface. This peak shift indicates that the surface relaxation reduces the energy of the electronic state of α-O. Because the valence band of TiO_2 consists of the filled states of oxygen atoms, this reduction of the energy of α-O gives rise to a larger surface band gap energy than that of the bulk.

Five nonlinear optical susceptibility elements $\chi_{S113}^{(2)(110)}$, $\chi_{S223}^{(2)(110)}$, $\chi_{S311}^{(2)(110)}$, $\chi_{S322}^{(2)(110)}$, and $\chi_{S333}^{(2)(110)}$ were calculated from the wavefunctions of the $TiO_2(110)$ surface by the *ab initio* calculation. The other components were zero due to the symmetry selection rules of the $TiO_2(110)$ 1×1 surface. Using these nonlinear and also linear optical susceptibility we have calculated SH intensity as shown in figures 14 and 15.

The measured SH intensity for the P_{in}/P_{out} polarization combination and for $k_{\parallel} \parallel$ [001] shown as empty circles in figure 14 is much larger than that for the S_{in}/P_{out} polarization combination and for $k_{\parallel} \parallel$ [001] shown as grey filled circles. The measured SH intensity for the two configurations increases sharply around the SH photon energy of $2\hbar\omega = 3.5$ eV. These features are mostly reproduced by the calculated SH intensity of the relaxed TiO$_2$(110) surface by a solid curve for the P_{in}/P_{out} polarization combination and by a dashed curve for the S_{in}/P_{out} polarization combination. However, we also notice that the experiment for the P_{in}/P_{out} polarization combination shows a gradual rise in SH intensity at lower energy than the calculation.

Figure 15 shows the calculated SH intensity patterns as a function of the sample rotation angle around the surface normal at the SH photon energy $2\hbar\omega = 4.0$ eV. The calculated results of the relaxed surface agree well with the experimental data in figures 4(e)–(h) from the viewpoints of both the shapes of angle patterns and the intensity ratios between different polarization combinations. Here we note that the calculated results of the unrelaxed surface did not reproduce the measured data at all.

We have also examined which of the Ti–O pairs on the TiO$_2$(110) surface dominantly contribute to the SH response. As shown in figure 1, the top surface of rutile TiO$_2$(110) consists of four atomic species, i.e. bridging oxygen (α), in-plane oxygen (β), 6-fold coordinated titanium (γ), and 5-fold coordinated titanium (δ). Accordingly, there are three pairs of Ti and O atoms adjacent to each other: α-O–γ-Ti, β-O–γ-Ti, and β-O–δ-Ti. We calculated the SH response from the electronic wavefunctions localized in each Ti–O pair. We found that the calculated pattern of the α-O–γ-Ti pair agreed with the measured pattern, while the other two calculated patterns did not. Furthermore, the calculated SH intensity of the α-O–γ-Ti pair was more than a few hundred times larger than those of the other pairs. Therefore, most of the SH intensity in the P_{in}/P_{out} polarization combination is judged to come from the α-O–γ-Ti pairs.

The fact that the calculated SH intensity patterns correctly predicted the experimental results means that not only the absolute value of the surface nonlinear susceptibility but also its phase has been calculated properly. This in turn indicates that the wavefunctions of the electrons at the TiO$_2$(110) surface have been calculated sufficiently well for the purposes of this study.

6. Discussion

6.1. Evaluation of the phenomenological analysis

The phenomenological analysis does not give a physical insight into the origin of the SH intensity, but clarifies dominant nonlinear susceptibility elements, and thus helps us to interpret the SH intensity spectra. The simultaneous numerical analysis of the (110) and (001) faces in the present study gives us the nonlinear susceptibility elements with less ambiguity than separate analyses for the two faces [14, 43]. However, there was still some arbitrariness in the obtained set of nonlinear susceptibility elements and we had to make several assumptions to get the susceptibility elements for physical discussion.

Nevertheless, the analysis at the SH photon energy of $2\hbar\omega = 4.66$ eV was quite successful. This fact indicates that at other photon energies such as at $2\hbar\omega = 3.34$ eV we could also determine the nonlinear susceptibility if we could measure the SH intensity patterns with better S/N ratio. In this work we used tunable nanosecond optical pulses, but if we could use picosecond pulses, the SH response would be stronger. Then we could even perform real time determination of the nonlinear susceptibility elements, while we scan the wavelength of the tunable light source, just as we do in the spectroscopic ellipsometry experiment.

It is very interesting that the higher-order bulk optical nonlinearity was observed through the fourfold symmetric component in the SH intensity patterns for the P_{in}/P_{out} and S_{in}/P_{out} polarization combinations in figure 5. However, the fourfold symmetric component in the SH intensity patterns does not dominate the signal intensity, and we cannot get detailed information on this bulk nonlinearity from the present result.

6.2. Origin of the SHG from the TiO₂(110) face

One of the biggest findings in this study is that the strong SH response to the electric field parallel to the [001] direction has been assigned to the surface contribution. From this fact and the discussion below we think that the SH intensity for this (110) face stems mainly from the Ti–O–Ti–O– chains on this surface.

Goniakowski and Gillan [44] have predicted that the surface bridging oxygen state is located at the top of the bulk valence band in the energy band diagram. This leads us to think that the observed upward two-photon transition may start from the bridging oxygen state because the SH photon energy in the present study is just above the bulk band gap energy of TiO₂. Then the electron will be successively excited by two photons of the same photon energy and reach the empty Ti state. These electronic transitions correspond to the electron movement from the α-O to γ-Ti in figure 1, i.e. within the Ti–O–Ti–O chains. This picture is also supported by the fact that in figure 4(a) the SH intensity from the TiO₂(110) face for the P_{in}/P_{out} polarization combination is large at the sample rotation angle $\phi = 0°$. At this sample rotation angle the incident electric field is parallel to the Ti–O–Ti–O– chain and thus the movement of the electron is induced within the chain. It has been generally pointed out that the Ti–O–Ti–O– chain is very important in designing nonlinear optical materials [45].

It is also interesting to find that the *ab initio* calculation at $2\hbar\omega = 4.0$ eV supports this model of resonant SH photon emission from Ti–O–Ti–O– chains consisting of α-O–γ-Ti pairs. Generally, we must be careful in adopting the results of theoretical calculations. However, in this study the *ab initio* calculation reproduces the experimental SH intensity patterns and spectra to a considerable extent. In such a case we feel that the *ab initio* calculation is quite reliable in predicting various linear and nonlinear optical properties of this surface. Though Ti and O atoms below the top surface also contribute to the total surface SH response, their contribution drastically decreases as they go deep into the bulk. Therefore, we conclude that the Ti–O–Ti–O– zigzag chains consisting of α-O and γ-Ti on the top surface dominantly contribute to the SH response of the TiO₂(110) surface.

6.3. SH intensity spectra of the Ti–O–Ti–O– chain

In this section we discuss the electronic states of the surface Ti–O–Ti–O– chain from the observed SH intensity spectra in figure 7. The electronic states we discuss in this photon energy region have not been treated well by photoemission or inverse photoemission spectroscopy [46–48].

In order to analyse the SH intensity spectra we further discuss the nonlinear susceptibility elements responsible for the SH intensity patterns in figure 4. In the SH intensity pattern analysis in section 4 we could not deduce which nonlinear susceptibility element is responsible for the variation of the SH intensity patterns for the S_{in}/P_{out} polarization combination in figures 4(c), (g), and (k). However, judging from the result of a separate experiment in section 3.1 that the SH intensity patterns for the S_{in}/P_{out} polarization combination are sensitive to the additive deposition of SiO₂ layers, we can say that the signals in this polarization combination come mainly from the surface. Then from the calculated patterns in figure 9, we

can say that the patterns for the $S_{\text{in}}/P_{\text{out}}$ polarization combination in figures 2(c) and (k) are dominated by the nonlinear susceptibility element $\chi_{S311}^{(2)(110)}$, and that in figure 2(g) is dominated by $\chi_{S322}^{(2)(110)}$.

For the discussion of the electronic states, we first note that the onset energy of the rise of the SH intensity is different between figures 7(a), (d), and (e). In the spectra in figures 7(a), (d), and (e), the dominant susceptibility element is suggested to be $\chi_{S113}^{(2)(110)}$, $\chi_{S311}^{(2)(110)}$, and $\chi_{S322}^{(2)(110)}$, respectively, from the above discussion. In figure 7(a) the onset energy is around 3.2 eV, while in figures 7(d) and (e) it is around 3.4 eV. The observed difference in the photon energy of the SH intensity rise between figures 2(a), (d) and (e) should reflect the difference in the electronic states or the electronic confinement in the Ti–O–Ti–O– zigzag chain. Here we model the Ti–O–Ti–O– zigzag chain as a quantum wire and consider the behaviour of the electron in this wire. In the second harmonic generation process described by the nonlinear susceptibility element of $\chi_{S113}^{(2)(110)}$ dominating the SH intensity in figure 7(a), the final transition dipole with frequency 2ω is induced in direction 1. In the second harmonic generation process described by the nonlinear susceptibility elements of $\chi_{S311}^{(2)(110)}$ and $\chi_{S322}^{(2)(110)}$ dominating the SH intensity in figures 7(d) and (e), respectively, the final transition dipole with frequency 2ω is induced in direction 3. The electronic wavefunction in the Ti–O–Ti–O– chain is delocalized in the direction of the chain axis (direction 1) but localized in the direction perpendicular to the chain axis (direction 3). Thus the transition energy should be smaller in the process described by $\chi_{S113}^{(2)(110)}$, as in figure 7(a), and larger in the process described by $\chi_{S311}^{(2)(110)}$ and $\chi_{S322}^{(2)(110)}$, as in figures 7(d) and (e). However, this feature is not seen in the calculated results by the *ab initio* method in figure 14. The clarification of this discrepancy will be our future problem.

It is also interesting to note that the spectrum in figure 7(d) is the upside-down image of the one in figure 7(e) in the photon energy region from 3.6 to 4.8 eV. This feature is consistent with the observed patterns in figures 4(c), (g), and (k). Namely, in these patterns the SH intensity is strong either at $\phi = 0°$ or $90°$ exclusively. This may be one feature of the energy spectrum of the electrons confined in a quantum wire. Namely, different modes of electronic oscillation may be exhibited in these two spectra. However, checking the validity of this guess will also be our future problem.

It is also interesting that the SH intensity spectrum of the TiO$_2$(001) face in figure 8 exhibits a lower onset energy of the SH intensity rise than any of the spectra in figure 7. As is pointed out in section 2.1, the structure of the TiO$_2$(001) face is not characterized in this study, so we have no idea about the origin of this difference. However, we can say at least that the TiO$_2$(001) face has an interface electronic state different from that of the TiO$_2$(110) face.

7. Conclusion

We have observed optical second harmonic generation (SHG) from the rutile H$_2$O/TiO$_2$(110) and (001) interfaces as a function of the sample rotation angle ϕ around its surface normal and the polarizations of incident and second harmonic light at different SH photon energies. Anisotropy in the nonlinear optical response from its surface and bulk depended strongly on the SH photon energy. In order to separate the contributions from various nonlinear susceptibility elements we have performed a numerical analysis of the SH intensity patterns as a function of ϕ from the TiO$_2$(110) and (001) faces simultaneously. We have found that the surface contribution is dominant at most of the measured photon energies, and the most dominant contribution in the $P_{\text{in}}/P_{\text{out}}$ polarization combination was the $\chi_{S113}^{(2)(110)}$ element. We have also obtained SH intensity spectra from the TiO$_2$(110) and (001) faces as a function of the SH photon energy. For interpreting these SH intensity spectra the results of the SH intensity

pattern analyses were used. We have found that the onset of the SH resonance of the $TiO_2(110)$ interface is $2\hbar\omega \sim 3.4$ eV with the nonlinear polarization at $2\hbar\omega$ perpendicular to the surface, while it is $2\hbar\omega \sim 3.2$ eV with the nonlinear polarization at $2\hbar\omega$ parallel to the [001] direction in the surface plane. *Ab initio* calculation by using the FLAPW method within the local-density approximation is shown to predict the SH intensity patterns and spectra correctly. The result that the SH intensity patterns were predicted fairly well indicates that the wavefunctions of the surface have been calculated sufficiently well for optical application. Also by using the calculated results, Ti–O–Ti–O– chains including the bridging oxygen atoms on the surface have been identified as the main origin of the SH radiation from the $TiO_2(110)$ surface.

Summarizing all these results, titanium dioxide has turned out to be a very good example for a consistent investigation of experiment, phenomenological theory and *ab initio* calculation of surface second harmonic radiation. The findings made in this paper will further give progress to studying the mechanisms of the photocatalytic, superhydrophilic, and biocompatible properties of this material.

Appendix

In this appendix we review a theoretical treatment of the reflected SH radiation from an anisotropic medium like rutile TiO_2. A similar treatment has been shown by several authors [13, 14]. So we only show the equations used in our calculation.

A.1. Linear reflection and refraction in an anisotropic medium

First, we show the equation for the internal field of the excitation beam in a dielectric structure in figure 3.

For the (110) face (model 1) it is

$$
\begin{pmatrix}
-\sin\phi & -\cos\theta\cos\phi & -e^\omega_{2o\downarrow x} & -e^\omega_{2e\downarrow x} & -e^\omega_{2o\uparrow x} & -e^\omega_{2e\uparrow x} & 0 & 0 \\
\cos\phi & -\cos\theta\sin\phi & -e^\omega_{2o\downarrow y} & -e^\omega_{2e\downarrow y} & -e^\omega_{2o\uparrow y} & -e^\omega_{2e\uparrow y} & 0 & 0 \\
\cos\theta\cos\phi & -\sin\phi & -a^\omega_{2o\downarrow x} & -a^\omega_{2e\downarrow x} & -a^\omega_{2o\uparrow x} & -a^\omega_{2e\uparrow x} & 0 & 0 \\
\cos\theta\sin\phi & \cos\phi & -a^\omega_{2o\downarrow y} & -a^\omega_{2e\downarrow y} & -a^\omega_{2o\uparrow y} & -a^\omega_{2e\uparrow y} & 0 & 0 \\
0 & 0 & e^\omega_{2o\downarrow x}e^{i\alpha^\omega_{2o}} & e^\omega_{2e\downarrow x}e^{i\alpha^\omega_{2e}} & e^\omega_{2o\uparrow x}e^{-i\alpha^\omega_{2o}} & e^\omega_{2e\uparrow x}e^{-i\alpha^\omega_{2e}} & -e^\omega_{3o\downarrow x}e^{i\alpha^\omega_{3o}} & -e^\omega_{3e\downarrow x}e^{i\alpha^\omega_{3e}} \\
0 & 0 & e^\omega_{2o\downarrow y}e^{i\alpha^\omega_{2o}} & e^\omega_{2e\downarrow y}e^{i\alpha^\omega_{2e}} & e^\omega_{2o\uparrow y}e^{-i\alpha^\omega_{2o}} & e^\omega_{2e\uparrow y}e^{-i\alpha^\omega_{2e}} & -e^\omega_{3o\downarrow y}e^{i\alpha^\omega_{3o}} & -e^\omega_{3e\downarrow y}e^{i\alpha^\omega_{3e}} \\
0 & 0 & a^\omega_{2o\downarrow x}e^{i\alpha^\omega_{2o}} & a^\omega_{2e\downarrow x}e^{i\alpha^\omega_{2e}} & a^\omega_{2o\uparrow x}e^{-i\alpha^\omega_{2o}} & a^\omega_{2e\uparrow x}e^{-i\alpha^\omega_{2e}} & -a^\omega_{3o\downarrow x}e^{i\alpha^\omega_{3o}} & -a^\omega_{3e\downarrow x}e^{i\alpha^\omega_{3e}} \\
0 & 0 & a^\omega_{2o\downarrow y}e^{i\alpha^\omega_{2o}} & a^\omega_{2e\downarrow y}e^{i\alpha^\omega_{2e}} & a^\omega_{2o\uparrow y}e^{-i\alpha^\omega_{2o}} & a^\omega_{2e\uparrow y}e^{-i\alpha^\omega_{2e}} & -a^\omega_{3o\downarrow y}e^{i\alpha^\omega_{3o}} & -a^\omega_{3e\downarrow y}e^{i\alpha^\omega_{3e}}
\end{pmatrix}
$$

$$
\times
\begin{pmatrix}
E^\omega_{rs0} \\
E^\omega_{rp0} \\
E^\omega_{2o\downarrow 0} \\
E^\omega_{2e\downarrow 0} \\
E^\omega_{2o\uparrow 0} \\
E^\omega_{2e\uparrow 0} \\
E^\omega_{3o\downarrow 0} \\
E^\omega_{3e\downarrow 0}
\end{pmatrix}
=
\begin{pmatrix}
-\cos\theta\cos\phi E^\omega_{inp0} + \sin\phi E^\omega_{ins0} \\
-\cos\theta\sin\phi E^\omega_{inp0} - \cos\phi E^\omega_{ins0} \\
\sin\phi E^\omega_{inp0} + \cos\theta\cos\phi E^\omega_{ins0} \\
-\cos\phi E^\omega_{inp0} + \cos\theta\sin\phi E^\omega_{ins0} \\
0 \\
0 \\
0 \\
0
\end{pmatrix}
\tag{A.1}
$$

where E^ω_{ri0} ($i =$ s, p) is the electric field amplitude of the reflected light of i-polarization in layer 1. It is defined by

$$\vec{E}_{\mathrm{rs}}^{\omega} = E_{\mathrm{rs0}}^{\omega} \begin{pmatrix} -\sin\phi \\ \cos\phi \\ 0 \end{pmatrix} e^{i\frac{\omega}{c}(\sin\theta\cos\phi\, x + \sin\theta\sin\phi\, y - \cos\theta\, z) - i\omega t} \tag{A.2}$$

$$\vec{E}_{\mathrm{rp}}^{\omega} = E_{\mathrm{rp0}}^{\omega} \begin{pmatrix} -\cos\theta\cos\phi \\ -\cos\theta\sin\phi \\ -\sin\theta \end{pmatrix} e^{i\frac{\omega}{c}(\sin\theta\cos\phi\, x + \sin\theta\sin\phi\, y - \cos\theta\, z) - i\omega t} \tag{A.3}$$

where $\vec{E}_{\mathrm{rs}}^{\omega}$ and $\vec{E}_{\mathrm{rp}}^{\omega}$ are the s- and p-polarized reflected electric fields, respectively. E_{ijk}^{ω} ($i = 2, 3$; $j = e, o$; $k = \ \downarrow, \uparrow$) is the electric field in the ith layer and is defined by

$$\vec{E}_{ijk}^{\omega} = E_{ijk0}^{\omega} \vec{e}_{ijk}^{\omega} e^{i\vec{k}_{ijk}^{\omega} \cdot \vec{r} - i\omega t}. \tag{A.4}$$

The suffices e and o denote the *extraordinary* and *ordinary* electromagnetic waves, respectively. The suffices $\downarrow$ and $\uparrow$ denote the downward and upward propagating waves, respectively. The vector $\vec{e}_{ijk}^{\omega}$ is the unit polarization vector of the electric field and can be written as

$$e_{iok}^{\omega} = \frac{1}{\sqrt{\varepsilon_{i\perp}^{\omega} - \sin^2\theta\cos^2\phi}} \begin{pmatrix} 0 \\ -\sqrt{\varepsilon_{i\perp}^{\omega} - \sin^2\theta} \\ \pm\sin\theta\sin\phi \end{pmatrix}$$
$$(+ \text{ and } - \text{ signs for } k = \ \downarrow \text{ and } \uparrow, \text{ respectively}) \tag{A.5}$$

$$e_{iek}^{\omega} = \frac{1}{\sqrt{\varepsilon_{i\parallel}^{\omega} + \left(\frac{\varepsilon_{i\parallel}^{\omega}}{\varepsilon_{i\perp}^{\omega}}\right) \sin^2\theta\cos^2\phi \left(\frac{\varepsilon_{i\parallel}^{\omega}}{\varepsilon_{i\perp}^{\omega}} - 1\right)}}$$
$$\times \begin{pmatrix} \sqrt{\varepsilon_{i\parallel}^{\omega}(1 - \frac{1}{\varepsilon_{i\perp}^{\omega}}\sin^2\theta\cos^2\phi)} \\ -\dfrac{\varepsilon_{i\parallel}^{\omega}\sin^2\theta\cos\phi\sin\phi}{\varepsilon_{i\perp}^{\omega}\sqrt{\varepsilon_{i\parallel}^{\omega}(1 - \frac{1}{\varepsilon_{i\perp}^{\omega}}\sin^2\theta\cos^2\phi)}} \\ \mp\dfrac{\varepsilon_{i\parallel}^{\omega}\sin\theta\cos\phi}{\varepsilon_{i\perp}^{\omega}\sqrt{\varepsilon_{i\parallel}^{\omega}(1 - \frac{1}{\varepsilon_{i\perp}^{\omega}}\sin^2\theta\cos^2\phi)}}\sqrt{\varepsilon_{i\parallel}^{\omega} - \sin^2\theta\sin^2\phi - \frac{\varepsilon_{i\parallel}^{\omega}}{\varepsilon_{i\perp}^{\omega}}\sin^2\theta\cos^2\phi} \end{pmatrix}$$
$$(- \text{ and } + \text{ signs for } k = \ \downarrow \text{ and } \uparrow, \text{ respectively}) \tag{A.6}$$

and $\vec{k}_{ijk}$ in equation (A.4) is defined by

$$\vec{k}_{iok}^{\omega} = \frac{\omega}{c} \begin{pmatrix} \sin\theta\cos\phi \\ \sin\theta\sin\phi \\ \pm\sqrt{\varepsilon_{i\perp}^{\omega} - \sin^2\theta} \end{pmatrix} \tag{A.7}$$

$$\vec{k}_{iek}^{\omega} = \frac{\omega}{c} \begin{pmatrix} \sin\theta\cos\phi \\ \sin\theta\sin\phi \\ \pm\sqrt{\varepsilon_{i\parallel}^{\omega} - \sin^2\theta\sin^2\phi - \frac{\varepsilon_{i\parallel}^{\omega}}{\varepsilon_{i\perp}^{\omega}}\sin^2\theta\cos^2\phi} \end{pmatrix}$$
$$(+ \text{ and } - \text{ signs for } k = \ \downarrow \text{ and } \uparrow, \text{ respectively}). \tag{A.8}$$

a_{ijkx}^{ω} and a_{ijky}^{ω} in the matrix elements in equation (A.1) are defined by

$$a_{ijkx}^{\omega} = \frac{c}{\omega}(k_{ijky}^{\omega} e_{ijkz}^{\omega} - k_{ijkz}^{\omega} e_{ijky}^{\omega}) \tag{A.9}$$

$$a_{ijky}^{\omega} = \frac{c}{\omega}(k_{ijkz}^{\omega} e_{ijkx}^{\omega} - k_{ijkx}^{\omega} e_{ijkz}^{\omega}) \tag{A.10}$$

and α_{ij}^{ω} is defined by

$$\alpha_{ij}^{\omega} = k_{ij\downarrow z}^{\omega} d \qquad (i = 2, 3, \ j = e, o). \tag{A.11}$$

For the (001) face (model 2) we can separate the discussion into those of s- and p-polarized field. The equation for the internal field is

$$
\begin{pmatrix}
1 & -e^{\omega}_{2s\downarrow y} & -e^{\omega}_{2s\uparrow y} & 0 \\
\cos\theta & -a^{\omega}_{2s\downarrow x} & -a^{\omega}_{2s\uparrow x} & 0 \\
0 & e^{\omega}_{2s\downarrow y}e^{ik^{\omega}_{2sz}d} & e^{\omega}_{2s\uparrow y}e^{-ik^{\omega}_{2sz}d} & -e^{\omega}_{3s\downarrow y}e^{ik^{\omega}_{3sz}d} \\
0 & a^{\omega}_{2s\downarrow x}e^{ik^{\omega}_{2sz}d} & a^{\omega}_{2s\uparrow x}e^{-ik^{\omega}_{2sz}d} & -a^{\omega}_{3s\downarrow x}e^{ik^{\omega}_{3sz}d}
\end{pmatrix}
\begin{pmatrix}
E^{\omega}_{rs0} \\
E^{\omega}_{2s\downarrow 0} \\
E^{\omega}_{2s\uparrow 0} \\
E^{\omega}_{3s\downarrow 0}
\end{pmatrix}
=
\begin{pmatrix}
-1 \\
\cos\theta \\
0 \\
0
\end{pmatrix}
E^{\omega}_{ins0}
\qquad (A.12)
$$

for s-polarized input. For p-polarized input

$$
\begin{pmatrix}
-\cos\theta & -e^{\omega}_{2p\downarrow x} & -e^{\omega}_{2p\uparrow x} & 0 \\
1 & -a^{\omega}_{2p\downarrow y} & -a^{\omega}_{2p\uparrow y} & 0 \\
0 & e^{\omega}_{2p\downarrow x}e^{ik^{\omega}_{2pz}d} & e^{\omega}_{2p\uparrow x}e^{-ik^{\omega}_{2pz}d} & -e^{\omega}_{3p\downarrow x}e^{ik^{\omega}_{3pz}d} \\
0 & a^{\omega}_{2p\downarrow y}e^{ik^{\omega}_{2pz}d} & a^{\omega}_{2p\uparrow y}e^{-ik^{\omega}_{2pz}d} & -a^{\omega}_{3p\downarrow y}e^{ik^{\omega}_{3pz}d}
\end{pmatrix}
\begin{pmatrix}
E^{\omega}_{rp0} \\
E^{\omega}_{2p\downarrow 0} \\
E^{\omega}_{2p\uparrow 0} \\
E^{\omega}_{3p\downarrow 0}
\end{pmatrix}
=
\begin{pmatrix}
-\cos\theta \\
-1 \\
0 \\
0
\end{pmatrix}
E^{\omega}_{inp0}.
$$
$$(A.13)$$

Here, E^{ω}_{ri0} ($i = $ s, p) is defined in equations (A.2) and (A.3). E^{ω}_{ijk} ($i = 2, 3$; $j = e, o$; $k = \downarrow, \uparrow$) is defined in equation (A.4). $\vec{e}^{\omega}_{ijk}$ is defined as

$$
\vec{e}^{\omega}_{isk} = \begin{pmatrix} 0 \\ 1 \\ 0 \end{pmatrix}
\qquad (A.14)
$$

$$
\vec{e}^{\omega}_{ipk} = \frac{1}{\sqrt{\varepsilon^{\omega}_{i\perp}[1 + \sin^2\theta(\varepsilon^{\omega}_{i\perp} - \varepsilon^{\omega}_{i\parallel})}}
\begin{pmatrix}
\sqrt{\varepsilon^{\omega}_{i\perp}(1 - \frac{\sin^2\theta}{\varepsilon^{\omega}_{i\parallel}})}\varepsilon^{\omega}_{i\parallel} \\
0 \\
\mp\sin\theta\varepsilon^{\omega}_{i\perp}
\end{pmatrix}
$$
$$(i, k) = (2, \downarrow), (2, \uparrow), \quad \text{and} \quad (3, \downarrow)$$
$$(- \text{ and } + \text{ signs for } k = \downarrow \text{ and } \uparrow, \text{ respectively}) \qquad (A.15)$$

and $\vec{k}^{\omega}_{ijk}$ is defined as

$$
\vec{k}^{\omega}_{isk} = \frac{\omega}{c}
\begin{pmatrix}
\sin\theta \\
0 \\
\pm\sqrt{\varepsilon^{\omega}_{i\perp} - \sin^2\theta}
\end{pmatrix}
\qquad (A.16)
$$

$$
\vec{k}^{\omega}_{ipk} = \frac{\omega}{c}
\begin{pmatrix}
\sin\theta \\
0 \\
\pm\sqrt{\varepsilon^{\omega}_{i\perp}(1 - \frac{\sin^2\theta}{\varepsilon^{\omega}_{i\parallel}})}
\end{pmatrix}.
\qquad (A.17)
$$

a^{ω}_{ijkx}, a^{ω}_{ijky}, and α^{ω}_{ij} are defined by (A.9) to (A.11) with $j = $ s, p.

A.2. SH electric field radiated from an anisotropic medium

We assume that the nonlinear polarization $\vec{P}^{NL}_0$ is induced in layer 2. The SH electric field in the dielectric structure described by model 1 can be written as

$$
\begin{pmatrix}
-\sin\phi & -\cos\theta\cos\phi & -e^{2\omega}_{2o\downarrow x} & -e^{2\omega}_{2e\downarrow x} & -e^{2\omega}_{2o\uparrow x} & -e^{2\omega}_{2e\uparrow x} & 0 & 0 \\
\cos\phi & -\cos\theta\sin\phi & -e^{2\omega}_{2o\downarrow y} & -e^{2\omega}_{2e\downarrow y} & -e^{2\omega}_{2o\uparrow y} & -e^{2\omega}_{2e\uparrow y} & 0 & 0 \\
\cos\theta\cos\phi & -\sin\phi & -a^{2\omega}_{2o\downarrow x} & -a^{2\omega}_{2e\downarrow x} & -a^{2\omega}_{2o\uparrow x} & -a^{2\omega}_{2e\uparrow x} & 0 & 0 \\
\cos\theta\sin\phi & \cos\phi & -a^{2\omega}_{2o\downarrow y} & -a^{2\omega}_{2e\downarrow y} & -a^{2\omega}_{2o\uparrow y} & -a^{2\omega}_{2e\uparrow y} & 0 & 0 \\
0 & 0 & e^{2\omega}_{2o\downarrow x}e^{i\alpha^{2\omega}_{2o}} & e^{2\omega}_{2e\downarrow x}e^{i\alpha^{2\omega}_{2e}} & e^{2\omega}_{2o\uparrow x}e^{-i\alpha^{2\omega}_{2o}} & e^{2\omega}_{2e\uparrow x}e^{-i\alpha^{2\omega}_{2e}} & -e^{2\omega}_{3o\downarrow x}e^{i\alpha^{2\omega}_{3o}} & -e^{2\omega}_{3e\downarrow x}e^{i\alpha^{2\omega}_{3e}} \\
0 & 0 & e^{2\omega}_{2o\downarrow y}e^{i\alpha^{2\omega}_{2o}} & e^{2\omega}_{2e\downarrow y}e^{i\alpha^{2\omega}_{2e}} & e^{2\omega}_{2o\uparrow y}e^{-i\alpha^{2\omega}_{2o}} & e^{2\omega}_{2e\uparrow y}e^{-i\alpha^{2\omega}_{2e}} & -e^{2\omega}_{3o\downarrow y}e^{i\alpha^{2\omega}_{3o}} & -e^{2\omega}_{3e\downarrow y}e^{i\alpha^{2\omega}_{3e}} \\
0 & 0 & a^{2\omega}_{2o\downarrow x}e^{i\alpha^{2\omega}_{2o}} & a^{2\omega}_{2e\downarrow x}e^{i\alpha^{2\omega}_{2e}} & a^{2\omega}_{2o\uparrow x}e^{-i\alpha^{2\omega}_{2o}} & a^{2\omega}_{2e\uparrow x}e^{-i\alpha^{2\omega}_{2e}} & -a^{2\omega}_{3o\downarrow x}e^{i\alpha^{2\omega}_{3o}} & -a^{2\omega}_{3e\downarrow x}e^{i\alpha^{2\omega}_{3e}} \\
0 & 0 & a^{2\omega}_{2o\downarrow y}e^{i\alpha^{2\omega}_{2o}} & a^{2\omega}_{2e\downarrow y}e^{i\alpha^{2\omega}_{2e}} & a^{2\omega}_{2o\uparrow y}e^{-i\alpha^{2\omega}_{2o}} & a^{2\omega}_{2e\uparrow y}e^{-i\alpha^{2\omega}_{2e}} & -a^{2\omega}_{3o\downarrow y}e^{i\alpha^{2\omega}_{3o}} & -a^{2\omega}_{3e\downarrow y}e^{i\alpha^{2\omega}_{3e}}
\end{pmatrix}
$$

$$\times \begin{pmatrix} E_{rs0}^{2\omega} \\ E_{rp0}^{2\omega} \\ E_{2o\downarrow 0}^{2\omega} \\ E_{2e\downarrow 0}^{2\omega} \\ E_{2o\uparrow 0}^{2\omega} \\ E_{2e\uparrow 0}^{2\omega} \\ E_{3o\downarrow 0}^{2\omega} \\ E_{3e\downarrow 0}^{2\omega} \end{pmatrix} = \begin{pmatrix} E_{IH0x} \\ E_{IH0y} \\ \frac{c}{2\omega}(k_{Sy}E_{IH0z} - k_{Sz}E_{IH0y}) \\ \frac{c}{2\omega}(k_{Sz}E_{IH0x} - k_{Sx}E_{IH0z}) \\ -e^{i\alpha_{IH}}E_{IH0x} \\ -e^{i\alpha_{IH}}E_{IH0y} \\ -\frac{c}{2\omega}(k_{Sy}E_{IH0z} - k_{Sz}E_{IH0y})e^{i\alpha_{IH}} \\ -\frac{c}{2\omega}(k_{Sz}E_{IH0x} - k_{Sx}E_{IH0z})e^{i\alpha_{IH}} \end{pmatrix}. \tag{A.18}$$

Here, $E_{rj0}^{2\omega}$, $E_{ijk0}^{2\omega}$, $\vec{e}_{ijk}^{2\omega}$, $\vec{k}_{ijk}^{2\omega}$, $a_{ijkx}^{2\omega}$, $a_{ijky}^{2\omega}$, and $\alpha_{ij}^{2\omega}$ are defined by equations (A.2)–(A.11) with ω replaced with 2ω. α_{IH} is defined by

$$\alpha_{IH} = k_{Sz}d \tag{A.19}$$

and $\vec{E}_{IH0}$ can be calculated from the equation

$$\begin{pmatrix} (k_{Sy}^2 + k_{Sz}^2) - \frac{4\omega^2}{c^2}\varepsilon_{2\parallel}^{2\omega} & -k_{Sx}k_{Sy} & -k_{Sx}k_{Sz} \\ -k_{Sx}k_{Sy} & (k_{Sx}^2 + k_{Sz}^2) - \frac{4\omega^2}{c^2}\varepsilon_{2\perp}^{2\omega} & -k_{Sy}k_{Sz} \\ -k_{Sx}k_{Sz} & -k_{Sy}k_{Sz} & (k_{Sx}^2 + k_{Sy}^2) - \frac{4\omega^2}{c^2}\varepsilon_{2\perp}^{2\omega} \end{pmatrix} \begin{pmatrix} E_{IH0x} \\ E_{IH0y} \\ E_{IH0z} \end{pmatrix}$$
$$= \frac{16\pi\omega^2}{c^2}\begin{pmatrix} P_{0x}^{NL} \\ P_{0y}^{NL} \\ P_{0z}^{NL} \end{pmatrix}. \tag{A.20}$$

The SH electric field in the dielectric structure described by model 2 can be written as

$$\begin{pmatrix} -\cos\theta & -e_{2p\downarrow x}^{\omega} & -e_{2p\uparrow x}^{\omega} & 0 \\ 1 & -a_{2p\downarrow y}^{\omega} & -a_{2p\uparrow y}^{\omega} & 0 \\ 0 & e_{2p\downarrow x}^{\omega}e^{ik_{2pz}^{\omega}d} & e_{2p\uparrow x}^{\omega}e^{-ik_{2pz}^{\omega}d} & -e_{3p\downarrow x}^{\omega}e^{ik_{3pz}^{\omega}d} \\ 0 & a_{2p\downarrow y}^{\omega}e^{ik_{2pz}^{\omega}d} & a_{2p\uparrow y}^{\omega}e^{-ik_{2pz}^{\omega}d} & -a_{3p\downarrow y}^{\omega}e^{ik_{3pz}^{\omega}d} \end{pmatrix} \begin{pmatrix} E_{rp0}^{\omega} \\ E_{2p\downarrow 0}^{\omega} \\ E_{2p\uparrow 0}^{\omega} \\ E_{3p\downarrow 0}^{\omega} \end{pmatrix} = \begin{pmatrix} E_{IH0x}^{2\omega} \\ H_{IH0y}^{2\omega} \\ -E_{IH0x}^{2\omega}e^{ik_{Sz}d} \\ -H_{IH0y}^{2\omega}e^{ik_{Sz}d} \end{pmatrix} \tag{A.21}$$

for the nonlinear polarization perpendicular to the plane of incidence.

$$\begin{pmatrix} 1 & -e_{2s\downarrow y}^{2\omega} & -e_{2s\uparrow y}^{2\omega} & 0 \\ \cos\theta & -a_{2s\downarrow x}^{2\omega} & -a_{2s\uparrow x}^{2\omega} & 0 \\ 0 & e_{2s\downarrow y}^{2\omega}e^{ik_{2sz}^{2\omega}d} & e_{2s\uparrow y}^{2\omega}e^{-ik_{2sz}^{2\omega}d} & -e_{3s\downarrow y}^{2\omega}e^{ik_{3sz}^{2\omega}d} \\ 0 & a_{2s\downarrow x}^{2\omega}e^{ik_{2sz}^{2\omega}d} & a_{2s\uparrow x}^{2\omega}e^{-ik_{2sz}^{2\omega}d} & -a_{3s\downarrow x}^{2\omega}e^{ik_{3sz}^{2\omega}d} \end{pmatrix} \begin{pmatrix} E_{rs0}^{2\omega} \\ E_{2s\downarrow 0}^{2\omega} \\ E_{2s\uparrow 0}^{2\omega} \\ E_{3s\downarrow 0}^{2\omega} \end{pmatrix} = \begin{pmatrix} E_{IH0y}^{2\omega} \\ H_{IH0x}^{2\omega} \\ E_{IH0y}^{2\omega}e^{ik_{Sz}d} \\ H_{IH0x}^{2\omega}e^{ik_{Sz}d} \end{pmatrix} \tag{A.22}$$

for the nonlinear polarization in the plane of incidence. Here, $E_{rj0}^{2\omega}$ is defined in equations (A.2) and (A.3) with $j = $ s, p. $E_{ijk0}^{2\omega}$ is defined in equation (A.4) with $j = $ s, p and with ω replaced with 2ω. $\vec{e}_{ijk}^{2\omega}$ is defined in equations (A.14) and (A.15) with ω replaced with 2ω. $\vec{k}_{ijk}^{2\omega}$ is defined in equations (A.16) and (A.17) with ω replaced with 2ω. Finally, $a_{ijkx}^{2\omega}$, $a_{ijky}^{2\omega}$, and $\alpha_{ij}^{2\omega}$ are defined by (A.9)–(A.11) with ω replaced with 2ω and with $j = $ s, p.

References

[1] McGilp J F 1999 *Surf. Rev. Lett.* **6** 529
[2] Heinz T F 1991 *Nonlinear Surface Electromagnetic Phenomena* ed H-E Ponath and G I Stegeman (Amsterdam: Elsevier) p 353

[3]   Shen Y R 1984 *The Principles of Nonlinear Optics* (New York: Wiley–Interscience) chapter 25

[4]   Shen Y R 1985 *J. Vac. Sci. Technol.* B **3** 1464

[5]   Yamada C and Kimura T 1993 *Phys. Rev. Lett.* **70** 2344

[6]   Yamada C and Kimura T 1994 *Phys. Rev.* B **49** 14372

[7]   Bottomley D J, Lüpke G, Mihaychuk J G and van Driel H M 1993 *J. Appl. Phys.* **74** 6072

[8]   Gridnev V N, Pavlov V V, Pisarev R V, Kirilyuk A and Rasing Th 2001 *Phys. Rev.* B **63** 184407

[9]   Stehlin T, Feller M, Guyot-Sionnest P and Shen Y R 1988 *Opt. Lett.* **13** 389

[10] Sipe J E, Moss D J and van Driel H M 1987 *Phys. Rev.* B **35** 1129

[11] Govorkov S V, Koroteev N I, Shumay I L and Yakovlev V V 1991 *J. Opt. Soc. Am.* B **8** 1023

[12] Bloembergen N 1992 *Nonlinear Optics* (Redwood City: Addison-Wesley) chapter 1

[13] Kumagai K, Mizutani G, Tsukioka H, Yamauchi T and Ushioda S 1993 *Phys. Rev.* B **48** 14488

[14] Kobayashi E, Mizutani G and Ushioda S 1997 *Japan. J. Appl. Phys.* **36** 7250

[15] Nakamura S, Matsuda K, Wakasugi T, Kobayashi E, Mizutani G, Ushioda S, Sekiya T and Kurita S 2000 *J. Lumin.* **87–89** 862

[16] Mizutani G, Ishibashi N, Nakamura S, Sekiya T and Kurita S 2001 *Int. J. Mod. Phys.* B **15** 3873

[17] Kobayashi E, Matsuda K, Mizutani G and Ushioda S 1999 *Surf. Sci.* **427/428** 294

[18] Vrillet G, Lee S K, McStay D and Robertson P K J 2004 *Appl. Surf. Sci.* **222** 33

[19] Kobayashi E, Wakasugi T, Mizutani G and Ushioda S 1998 *Surf. Sci.* **402–404** 537 Later we found that there was a small amount of Si contamination on the sample surfaces used in papers 14 and 19, so that some of the SH intensity patterns in figure 4 in the present paper should replace the corresponding patterns in these papers.

[20] Sano H, Mizutani G, Wolf W and Podloucky R 2004 at press

[21] Asari E, Hayami W and Souda R 2000 *Appl. Surf. Sci.* **167** 169

[22] Onishi H and Iwasawa Y 1994 *Surf. Sci.* **313** L783

[23] Chung Y W, Lo W J and Somorjai G A 1977 *Surf. Sci.* **64** 588

[24] Henderson M A 1996 *Surf. Sci.* **355** 151

[25] Diebold U 2003 *Surf. Sci. Rep.* **48** 53

[26] Guyot-Sionnest P, Chen W and Shen Y R 1986 *Phys. Rev.* B **33** 8254

[27] Sano H and Mizutani G 2003 *e-J. Surf. Sci. Nanotechnol.* **1** 57

[28] Glassford K M and Chelikowsky J R 1992 *Phys. Rev.* B **46** 1284

[29] Mo S-D and Ching W Y 1995 *Phys. Rev.* B **51** 13023

[30] Vogtenhuber D, Podloucky R, Neckel A, Steinemann S G and Freeman A J 1994 *Phys. Rev.* B **49** 2099

[31] Ramamoorthy M, Vanderbilt D and King-Smith R D 1994 *Phys. Rev.* B **49** 16721

[32] Reinhardt P and Hess B A 1994 *Phys. Rev.* B **50** 12015

[33] Bates S P, Kresse G and Gillan M J 1997 *Surf. Sci.* **385** 386

[34] Schelling P K, Yu N and Halley J W 1998 *Phys. Rev.* B **58** 1279

[35] Harrison N M, Wang X-G, Muscat J and Scheffler M 1999 *Faraday Discuss.* **114** 305

[36] Sano H, Mizutani G, Wolf W and Podloucky R 2002 *Phys. Rev.* B **66** 195338

[37] Hedin L and Lundqvist B I 1971 *J. Phys. C: Solid State Phys.* **4** 2064

[38] Reining L, Del Sole R, Cini M and Ping J G 1994 *Phys. Rev.* B **50** 8411

[39] Mendoza B S, Gaggiotti A and Del Sole R 1998 *Phys. Rev. Lett.* **81** 3781

[40] Murao M, Kobayashi E and Mizutani G 2001 *Technical Digest of CLEO/Pacific Rim 2001* (Hawaii: Optical Society of America) pp II146–7

[41] Grant F A 1959 *Rev. Mod. Phys.* **31** 646

[42] Ribarsky M W 1985 *Handbook of Optical Constants of Solids* ed E D Palik (San Diego, CA: Academic) p 795

[43] Tom H W K, Heinz T F and Shen Y R 1983 *Phys. Rev. Lett.* **51** 1983

[44] Goniakowski J and Gillan M J 1996 *Surf. Sci.* **350** 145

[45] Gopalakrishnan J, Ramesha K, Rangan K K and Pandey S 1999 *J. Solid State Chem.* **148** 75

[46] Heise R, Courths R and Witzel S 1992 *Solid State Commun.* **84** 599

[47] Hardman P J, Raikar G N, Muryn C A, van der Laan G, Wincott P L, Thornton G, Bullett D W and Dale P A D M A 1994 *Phys. Rev.* B **49** 7170

[48] See A K, Thayer M and Bartynski R A 1993 *Phys. Rev.* B **47** 13722